Small intestine and colon tissue-resident memory CD8+ T cells exhibit molecular heterogeneity and differential dependence on Eomes

Yun Hsuan Lin[1,6], **Han G. Duong**[1,6], **Abigail E. Limary**[1,6], **Eleanor S. Kim**[1,6], **Paul Hsu**[1], **Shefali A. Patel**[1], **William H. Wong**[1], **Cynthia S. Indralingam**[1], **Yi Chia Liu**[1], **Priscilla Yao**[1], **Natalie R. Chiang**[1], **Sara A. Vandenburgh**[1], **Taylor R. Anderson**[1], **Jocelyn G. Olvera**[1], **Amir Ferry**[2], **Kennidy K. Takehara**[2], **Wenhao Jin**[3], **Matthew S. Tsai**[1], **Gene W. Yeo**[3,4], **Ananda W. Goldrath**[2], **John T. Chang**[1,5,7,*]

[1]Department of Medicine, University of California San Diego, La Jolla, CA 92093, USA

[2]Division of Biological Sciences, University of California San Diego, La Jolla, CA 92093, USA

[3]Department of Cellular and Molecular Medicine, University of California San Diego, La Jolla, CA 92093, USA

[4]Institute for Genomic Medicine, University of California San Diego, La Jolla, CA 92093, USA

[5]Department of Medicine, Jennifer Moreno Department of Veteran Affairs Medical Center, San Diego, CA 92161, USA

[6]These authors contributed equally

[7]Lead contact

SUMMARY

Tissue-resident memory CD8+ T (T_{RM}) cells are a subset of memory T cells that play a critical role in limiting early pathogen spread and controlling infection. T_{RM} cells exhibit differences across tissues, but their potential heterogeneity among distinct anatomic compartments within the small intestine and colon has not been well-recognized. Here, by analyzing T_{RM} cells from the lamina propria and epithelial compartments of the small intestine and colon, we showed that intestinal T_{RM} cells exhibited distinctive patterns of cytokine and granzyme expression, along with

DECLARATION OF INTERESTS

substantial transcriptional, epigenetic, and functional heterogeneity. The T-box transcription factor Eomes, which represses T_{RM} cell formation in some tissues, exhibited unexpected context-specific regulatory roles in supporting the maintenance of established T_{RM} cells in the small intestine, but not in the colon. Taken together, these data provide previously unappreciated insights into the heterogeneity and differential requirements for the formation vs. maintenance of intestinal T_{RM} cells.

eTOC Blurb

The tissue- and context-specific regulation of tissue-resident memory T (T_{RM}) cells, which provide protection in organs and at barrier sites, is an emerging concept. Lin, Duong, Limary, Kim, et al. show that CD8$^+$ T_{RM} cells from SI vs. colon exhibit unique molecular and functional attributes along with distinct transcriptional requirements for their maintenance.

Graphical Abstract
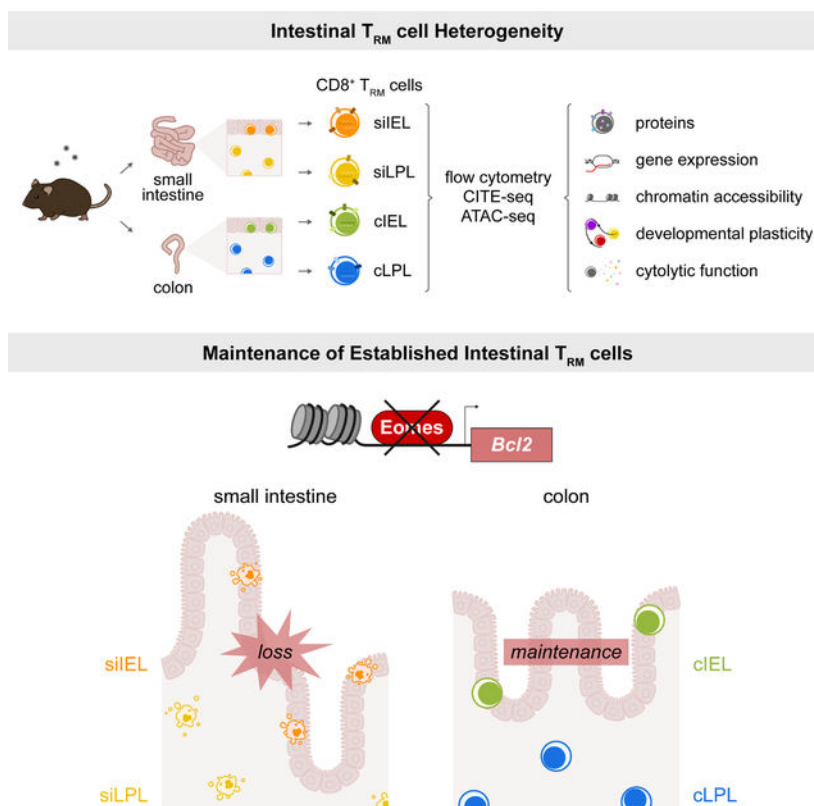
Keywords

Tissue-resident memory CD8$^+$ T cells; small intestine; colon; single-cell RNA-sequencing; single-cell ATAC-sequencing; Eomes

INTRODUCTION

During a microbial infection, CD8^{+} T cells give rise to short-lived effector cells that provide acute host defense and long-lived memory cells that provide sustained protection[1]. Memory CD8^{+} T cells can be broadly classified as circulating and tissue-resident memory (T_{RM}) cells, with circulating memory T cells further subdivided into central memory (T_{CM}), effector memory (T_{EM}), terminal effector memory (t-T_{EM}), and peripheral memory (T_{PM}) cells, based on distinct phenotypic, homeostatic, functional, and migratory properties[2–4]. T_{RM} cells are so named because they tend to 'reside' in the tissue in which they form, though it is now clear that T_{RM} cells can egress into the circulation after reactivation[5,6]. T_{RM} cells are a distinct component of the memory T cell compartment that play a crucial role in host defense against microbial pathogens, particularly infections at barrier sites, owing to their immediate effector capabilities and positioning in tissues[7–10]. Moreover, cells with T_{RM}-like characteristics play crucial roles in mediating immune responses against tumors[11–13]. Conversely, T cells exhibiting a T_{RM}-like phenotype can mediate pathology in autoimmune and inflammatory disorders[14–17].

Early studies sought to identify shared features of T_{RM} cells distinct from circulating memory cells, including increased expression of molecules necessary for trafficking to and retention in tissues, such as CD69 and αEβ7 integrin; decreased expression of molecules that promote egress to the circulation, such as the chemokine receptor CCR7, the receptor for sphingosine 1-phosphate (S1PR1), and the transcription factor KLF2[9,18,19]; and induction of transcription factors that establish the tissue residency program, including Blimp1, Hobit, and Runx3[11,20]. However, substantial transcriptional and functional heterogeneity exists among T_{RM} cells derived from different tissues[5,21–23], with T_{RM} cells from disparate tissues exhibiting unique requirements for their formation. For example, Hobit is required for T_{RM} cell formation in the skin, liver, and small intestine intraepithelial (siIEL) and lamina propria (siLPL) compartments[20], but not in the lung[24]. IL-15 signaling is required for the formation of T_{RM} cells in the skin, liver, salivary gland, and kidney, but not in the pancreas, female reproductive tract, or the siIEL and siLPL compartments[18,25–27].

While the signals required for T_{RM} cell formation are a focus of current research, the requirements for the maintenance of established T_{RM} cells are less understood. The costimulatory molecule ICOS promotes the formation of T_{RM} cells in the kidney, salivary gland, and siIEL and siLPL compartments, but is not required for their maintenance[28]. This illustrates the underappreciated concept that factors required for T_{RM} cell formation may be distinct from those required for their maintenance. Moreover, the mechanisms underlying T_{RM} cell formation and maintenance may be distinct across tissues. Lastly, it should be emphasized that conclusions based on siIEL T_{RM} cells, which have been studied extensively, are typically generalized to all intestinal T_{RM} cells, even though there is a paucity of work involving siLPL T_{RM} cells[20,28–30]. Moreover, T_{RM} cells from the colon IEL (cIEL) and LPL (cLPL) compartments have not been previously investigated in depth.

Here we performed an extensive comparative analysis of T_{RM} cells from the siIEL, siLPL, cIEL and cLPL intestinal tissue compartments. Intestinal T_{RM} cells exhibited heterogeneity

in their expression of the widely used T_{RM} cell markers CD69 and CD103, along with distinctive patterns of cytokine and granzyme expression. For example, siIEL T_{RM} cells expressed the highest levels of GzmA and GzmB, whereas cIEL T_{RM} cells exhibited the greatest capacity for IFNγ and TNF production. Furthermore, our studies revealed substantial transcriptional, epigenetic, and functional heterogeneity among T_{RM} cells from the siIEL, siLPL, ciIEL, and cLPL compartments. We elucidated unexpected tissue- and context-specific regulatory roles for the T-box transcription factor Eomesodermin (Eomes), previously known to repress T_{RM} cell formation in the skin, liver, and kidney[31,32]. We ascertained a role for Eomes in supporting the maintenance of established T_{RM} cells in the small intestine (SI), but not in the colon, in part by inducing the anti-apoptotic molecule Bcl-2. Taken together, these data provide previously unappreciated insights into the heterogeneity and differential requirements for the formation vs. maintenance of T_{RM} cells from the SI and colon.

RESULTS

Phenotypic and functional heterogeneity among CD8+ T_{RM} cells in the SI and colon.

The current understanding of 'intestinal' CD8+ T_{RM} cells is primarily focused on those that form in the siIEL compartment, even though T_{RM} cells also form in the siLPL[29,30], cIEL, and cLPL compartments[33]. Thus, in order to directly compare CD8+ T_{RM} cells from each of these four intestinal tissue compartments under the same experimental conditions, CD8+CD45.1+ P14 T cells, which have transgenic expression of a T cell receptor (TCR) that recognizes an immunodominant epitope of lymphocytic choriomeningitis virus (LCMV), were adoptively transferred into congenic CD45.2+ recipients that were subsequently infected intraperitoneally (i.p.) with the Armstrong strain of LCMV (Figure 1A). We analyzed donor P14 T cells from the spleens and the four intestinal tissue compartments of recipient mice after 21 days post-infection. To exclude circulating cells, anti-CD8α antibodies were injected intravenously (i.v.) into recipient mice 3–5 minutes prior to sacrifice and only 'i.v.-negative' cells were considered tissue-resident for subsequent downstream analyses[34]. We observed that siIEL and siLPL T_{RM} cells were the most abundant intestinal T_{RM} cells, followed by cLPL T_{RM} cells, with cIEL T_{RM} cells representing the least abundant intestinal T_{RM} cells (Figures 1B and S1A), consistent with previously published results using a microscopy-based quantification method[33].

In addition to being a marker of early T cell activation, CD69 is often considered a marker for T_{RM} cells in many tissues, whereas CD103 is expressed by T_{RM} cells only in certain tissues with an epithelial component, such as in the skin and siIEL compartment[7,9]. In agreement with previously published data[9], we observed that the vast majority of siIEL CD8+ T_{RM} cells expressed high levels of both CD69 and CD103 (Figure 1C). By contrast, we observed that CD8+ T_{RM} cells in the other three intestinal compartments were highly heterogeneous with respect to CD69 and CD103 expression. Approximately 60% of siLPL T_{RM} cells, and far fewer ciIEL and cLPL T_{RM} cells, expressed both CD69 and CD103 (Figure 1C); most siLPL and cLPL T_{RM} cells expressed only CD69, and a proportion of cIEL and cLPL T_{RM} cells expressed neither CD69 nor CD103 (Figure 1C). Since CD103 (integrin αE) can pair with different β integrins, we examined the expression of several

integrin heterodimers and chemokine receptors. The expression patterns of integrin αEβ7 (CD103/β7) by T_{RM} cells paralleled those observed for CD103 alone, with the highest levels in the siIEL compartment and progressively lower levels in the siLPL, cIEL, and cLPL compartments (Figure 1D), indicating that the levels of CD103 observed indeed reflected αEβ7 integrin expression. Few T_{RM} cells expressed integrin α4β7 (CD49d/β7), but a greater proportion of IEL T_{RM} cells expressed α4β7 integrin compared to LPL T_{RM} cells (Figure 1E). A larger proportion of colon T_{RM} cells expressed α1β1 (CD49a/β1) and α4β1 (CD49d/β1) integrins compared to SI T_{RM} cells (Figures 1F and 1G). Compared to T_{RM} cells in the other intestinal tissue compartments, a higher proportion of cIEL T_{RM} cells tended to express CXCR3, CXCR4, and CCR6, and exhibited higher levels of these molecules on a per-cell basis (Figures 1H–1J). Compared to naïve and circulating memory T cells, intestinal T_{RM} cells expressed lower levels of CCR9, but a greater proportion of cLPL T_{RM} cells expressed CCR9 compared to T_{RM} cells from the other intestinal compartments (Figure 1K).

Having established that T_{RM} cells from the four intestinal tissue compartments exhibited phenotypic heterogeneity, we next sought to determine whether intestinal T_{RM} cells demonstrated functional differences. Most siIEL T_{RM} cells expressed the highest levels of GzmA and GzmB on a per-cell basis (Figures 2A and 2B). Small intestine LPL and cLPL T_{RM} cells expressed low levels of GzmA but higher levels of GzmB, whereas cIEL T_{RM} cells expressed relatively low levels of both granzymes. Few T_{RM} cells were capable of IL-2 production, but T_{RM} cells from all four intestinal compartments were capable of producing TNF, with the highest per-cell amounts produced by cIEL T_{RM} cells (Figures 2C and 2D). T_{RM} cells from the IEL compartments tended to produce higher levels of IFNγ compared to LPL T_{RM} cells, with the highest levels of IFNγ produced by cIEL T_{RM} cells on a per-cell basis; moreover, the vast majority of cIEL T_{RM} cells were capable of producing IFNγ (Figure 2E). Colon IEL T_{RM} cells were capable of the greatest polyfunctionality, followed by siIEL T_{RM} cells (Figure 2F). This functional heterogeneity among intestinal T_{RM} cells did not appear to be primarily driven by differences in CD69 and CD103 expression (Figures S1B–G). Lastly, we observed that siIEL and siLPL T_{RM} cells exhibited greater longevity than cIEL and cLPL T_{RM} cells, comparable to that of T_{CM} cells (Figure 2G).

We next examined levels of cytokine and signaling receptors that have been previously associated with circulating and tissue-resident memory CD8^{+} T cells[1]. T_{RM} cells from all four intestinal tissue compartments expressed similar levels of CD127 (IL-7Rα) (Figure 2H). By contrast, a higher proportion of colon T_{RM} cells expressed CD122 (IL-2Rβ) compared to SI T_{RM} cells; among all intestinal T_{RM} cells, cIEL T_{RM} cells exhibited the highest proportions expressing CD122 (Figure 2I). CD27, a costimulatory receptor that has been associated with circulating memory T cells, was expressed at lower levels by intestinal T_{RM} cells compared to circulating memory cells; however, among intestinal T_{RM} cells, a higher proportion of cIEL T_{RM} cells expressed CD27 compared to cells from the other three compartments (Figure 2J). Taken together, these results indicated that T_{RM} cells from the four intestinal compartments exhibit previously unappreciated phenotypic and functional heterogeneity.

Single-cell transcriptomic, epigenetic, and protein profiling reveal potential regulators of intestinal T_{RM} cell heterogeneity.

To elucidate inter- and intra-intestinal T_{RM} cell heterogeneity, we performed Cellular Indexing of Transcriptomes and Epitopes (CITE-seq), which enables measurement of proteins and the transcriptome at the single-cell level[35]. CD45.1$^+$ P14 T cells were adoptively transferred into CD45.2$^+$ recipients prior to infection with LCMV. After 30 days post-infection, P14 T cells from each intestinal tissue compartment were isolated by FACS and processed for CITE-seq using the 10x Genomics platform. Antibodies targeting 50 proteins, some of which have previously implicated in CD8$^+$ T cell activation and differentiation, were selected for inclusion in the CITE-seq antibody panel (STAR Methods).

Uniform Manifold Approximation and Projection (UMAP) analyses revealed that while T_{RM} cells from each intestinal tissue compartment clustered distinctly, siIEL and siLPL T_{RM} cells clustered more closely together, whereas cIEL and cLPL T_{RM} cells clustered more closely together (Figure S2A). We also observed additional heterogeneity within and among T_{RM} cells from each intestinal tissue compartment; intestinal T_{RM} cells separated into 15 clusters exhibiting disparate gene expression patterns (Figures S2A–S2C, Tables S1 and S2), with colon T_{RM} cells predominantly contained within clusters 4, 5, 6, and 14, and SI T_{RM} cells found within the remaining clusters. Pathway analyses[36] of the clusters revealed that certain pathways, such as TCR signaling, were enriched in T_{RM} cells across all clusters, while others, such as pathways regulating the cell cycle, were preferentially enriched in T_{RM} cells from certain clusters (Figure S2D, Table S2).

Next we analyzed T_{RM} cells from each of the four intestinal tissues as 'pseudo-bulk' samples in order to uncover the most substantial differences among T_{RM} cells from each intestinal tissue compartment. Intestinal T_{RM} cells exhibited numerous transcriptional disparities, with siIEL, siLPL, cIEL, and cLPL T_{RM} cells exhibiting 605, 314, 754, and 723 differentially expressed genes, respectively (Figures 3A and 3B, Table S3). Focusing next on specific genes, we observed that SI T_{RM} cells expressed higher levels of cytolytic molecules and certain surface receptors such as *Cd160* (Figure 3B). By contrast, colon T_{RM} cells expressed higher levels of transcripts encoding for killer lectin receptors and a number of surface receptors, including *Il18r1*, *Ly6c*, *Il6ra*, *Ifngr1*, and *Slamf6* (Figure 3B). With respect to transcription factors, SI T_{RM} cells expressed higher levels of factors previously implicated in siIEL T_{RM} cell differentiation, such as *Ahr*, *Prdm1* (Blimp1*)*, *Runx3*, *P2rx7*, and *Zfp683* (Hobit)[11,20,37–39]; conversely, colon T_{RM} cells expressed higher levels of transcription factors previously associated with circulating memory T cells, including *Tcf7* and *Lef1*[40,41]. Compared to IEL T_{RM} cells, LPL T_{RM} cells tended to express higher levels of *Areg* and *Rorc,* while cIEL T_{RM} cells expressed the highest levels of several transcription factors, including *Bach2* (Figure 3B). Colon IEL T_{RM} cells also expressed the highest levels of *Eomes*, an unexpected finding since the expression of Eomes has been previously shown to be extinguished during the differentiation of skin T_{RM} cells[31].

Analyses of protein expression from the CITE-seq antibody panel (Figures 3C and 3D) along with independent flow cytometry experiments (Figures 3E–3I and S3C–S3H) confirmed some of the key findings observed at the transcriptional level. For example, colon T_{RM} cells expressed higher levels of proteins such as Ly108 (SLAMF6) and Ly6C, whereas

SI T_{RM} cells expressed higher levels of proteins such as CD38, CD160, and P2RX7. Small intestine IEL T_{RM} cells expressed the highest levels of CD103 and integrin β7; siLPL T_{RM} cells expressed the highest levels of TIGIT, CD5, and CD270 (HVEM); and cIEL T_{RM} cells expressed the highest levels of several proteins, such as CD314 (NKG2D) and CD44. The T-box transcription factor T-bet was detectable at low levels in intestinal T_{RM} cells (Figure 3G). Eomes was detectable in all intestinal T_{RM} cells (Figure 3H), but expressed by a higher proportion of colon T_{RM} cells compared to SI T_{RM} cells; among colon T_{RM} cells, a higher proportion of cIEL T_{RM} cells expressed Eomes protein compared to cLPL T_{RM} cells, consistent with the transcriptional data (Figure 3B).

To investigate whether the transcriptional disparities among T_{RM} cells from the four intestinal compartments were accompanied by epigenetic heterogeneity, we performed the assay for transposase-accessible chromatin with high-throughput sequencing at the single-cell level (scATAC-seq). UMAP analyses revealed that intestinal CD8$^+$ T_{RM} cells clustered distinctly based on differential chromatin accessibility (Figures S4A and S4B, Table S4). Additional analyses revealed 39, 23, 110, and 257 transcription factor binding motifs that were preferentially enriched within differentially accessible chromatin peaks in siIEL, siLPL, cIEL, and cLPL T_{RM} cells, respectively (Figure S4C, Tables S5 and S6). For example, motifs for *Ahr* and basic helix-loop-helix family transcription factors, such as *Hes1*, *Hes2*, and *Bhlhe40*, were enriched in siIEL T_{RM} cells (Figure S4D, Table S6), while motifs for IRF family members (*Irf2, Irf3, Irf7, Irf8*) were enriched in siLPL T_{RM} cells (Figure S4E). Moreover, motifs for ROR/RAR family members, including *Rora* and *Rarb*, were enriched in cLPL T_{RM} cells (Figure S4G), whereas motifs for a number of T-box transcription factor family members, including *Tbx21* and *Eomes*, were enriched in ciIEL T_{RM} cells (Figure S4F). We also identified transcription factor binding motifs that were shared between T_{RM} cells from different intestinal tissue compartments, such as *Runx3* for siIEL and cIEL T_{RM} cells, *Nfatc1* for siLPL and cLPL T_{RM} cells, and *Hic1* for cIEL and cLPL T_{RM} cells (Figures S4H–S4J). Taken together, these findings reveal previously unappreciated phenotypic, transcriptional, and epigenetic heterogeneity among intestinal T_{RM} cells.

Small intestine IEL and LPL T_{RM} cells may exhibit differences in developmental plasticity.

We next sought to determine whether T_{RM} cells from the intestinal tissue compartments exhibited disparities in developmental plasticity, as has been reported for T_{RM} cells from other tissues[21,22]. Using the single-cell RNA-seq data, we first inferred the differentiation trajectories of siIEL and siLPL T_{RM} cells by applying scVelo, a previously published framework to analyze transcriptional dynamics of splicing kinetics using a likelihood-based dynamical model[42,43]. These analyses predicted that although most siIEL and siLPL T_{RM} cells followed similar differentiation paths, several subpopulations of siLPL T_{RM} cells clustered distinctly from siIEL T_{RM} cells (Figure 4A). These clusters of siLPL TRM cells were projected later in 'latent time,' an approximation of real time experienced by cells as they undergo differentiation (Figure 4B). These results raised the possibility that these siLPL T_{RM} cell clusters may be more differentiated and exhibit less developmental plasticity than siIEL T_{RM} cells, though it should be noted that trajectories, velocities, and pseudotime distributions inferred by scVelo and other single-cell trajectory inference methods may not

always be aligned with real time. Thus, to test this prediction experimentally, CD45.1$^+$ P14 T cells were adoptively transferred into CD45.2$^+$ recipients subsequently infected with LCMV (Figure 4C). After day 21 post-infection, CD45.1$^+$ P14 T cells from the siIEL or siLPL compartments ('ex-siIEL' or 'ex-siLPL') were FACS-purified and adoptively transferred into separate naïve CD45.2$^+$ recipients subsequently infected with LCMV. Ten to 14 days later, we analyzed donor 'ex-siIEL' or 'ex-siLPL' P14 T cells from the spleens and the four intestinal tissue compartments of recipient mice. Compared to ex-siLPL T$_{RM}$ cells, ex-siIEL T$_{RM}$ cells appeared to be superior in their ability to give rise to secondary T$_{RM}$ cells in the siIEL and siLPL compartments. Moreover, compared to ex-siLPL T$_{RM}$ cells, ex-siIEL T$_{RM}$ cells tended to have an increased ability to give rise to secondary T$_{RM}$ cells in the colon and secondary memory cells in the spleen (Figures 4D–4F). Ex-siIEL T$_{RM}$ cells that gave rise to secondary T$_{RM}$ cells tended to adopt the phenotypic characteristics of their new environments. For example, ex-siIEL T$_{RM}$ cells that gave rise to secondary cLPL T$_{RM}$ cells no longer exhibited a CD69$^+$CD103$^+$ phenotype (Figure 4G) and instead expressed low levels of GzmA and high levels of Ly6C (Figures 4H and 4I), both distinctive features of primary cLPL T$_{RM}$ cells identified above (Figures 1C, 2A, 3C, 3D, and 3E). Lastly, ex-siIEL T$_{RM}$ cells gave rise to secondary T$_{EM}$ cells in the spleen, but not secondary T$_{CM}$ cells (Figure 4J), consistent with previously published data[21]. Taken together, these findings suggest that T$_{RM}$ cells from different anatomic regions within the same organ may exhibit disparate degrees of developmental plasticity.

Eomes is dispensable for initial formation of intestinal CD8$^+$ T$_{RM}$ cells, but plays a critical role in the maintenance of established SI CD8$^+$ T$_{RM}$ cells.

The unexpected observation that Eomes was more highly expressed in colon T$_{RM}$ cells compared to those in the SI (Figures 3B and 3H) raised the possibility that Eomes might play a role in intestinal T$_{RM}$ cells that is distinct from its previously established role in skin, liver, and kidney T$_{RM}$ cells[31,32]. To evaluate whether Eomes plays a role in the initial formation of CD8$^+$ T$_{RM}$ cells in each of the four intestinal tissue compartments, congenically distinct control and *Eomes*$^{fl/fl}$*Cd4*^{Cre} (Eomes conditional (c)KO) P14 T cells were adoptively transferred at a 1:1 ratio into recipient mice subsequently infected with LCMV (Figure 5A) and analyzed at day 7 and after 21 days post-infection. The proportions and absolute numbers of splenic and intestinal Eomes cKO P14 T cells were not substantially different than those of control cells at 7 days post-infection (Figures 5B, S5A–S5C, and S6A). However, the proportions of Eomes cKO CD69$^+$CD103$^+$ P14 T cells were increased in each of the four intestinal tissue compartments (Figure 5C). In line with these observations, forced Eomes expression resulted in reduced proportions of CD69$^+$CD103$^+$ T cells in each of the four intestinal tissue compartments (Figure S6B). Compared to control counterparts, intestinal Eomes cKO CD8$^+$ P14 T cells exhibited modest differences in the expression of cytolytic granules, markers of proliferation (Ki67), cytokines, and T-bet (Figures S6C–S6H). Splenic Eomes cKO CD8$^+$ P14 T cells exhibited a decrease in the proportion of cells exhibiting a terminal effector phenotype (KLRG1^{hi}CD127^{lo}) and a slight increase in the proportion of cells exhibiting a memory precursor phenotype (KLRG1^{lo}CD127^{hi}) phenotype, along with a modest decrease in GzmA expression (Figures S5D–S5I).

Analyses performed after day 21 post-infection demonstrated similar proportions and absolute numbers of intestinal control and Eomes cKO P14 T cells (Figure 5D), along with similar proportions of CD69+CD103+ cells (Figure 5E) and expression patterns of granzymes and cytokines (Figures S6I and S6J). In the spleen, although the numbers of total circulating memory cells were unchanged by the absence of Eomes (Figure S5J), the proportion of T_{CM} (CD62L^{hi}CD127^{hi}) cells was decreased with a corresponding increase in the proportion of T_{EM} (CD62L^{lo}CD127^{hi}) cells (Figure S5K). The reduced proportion of Eomes cKO T_{CM} cells was associated with decreased expression of CD122, a known target of Eomes in circulating CD8+ T cells[44], along with increased expression of T-bet by T_{CM} cells (Figures S5L and S5M). Taken together, these findings indicate that Eomes is largely dispensable for CD8+ T_{RM} cell formation in the four intestinal tissue compartments. Although Eomes does appear to play a role in repressing CD69 and CD103 expression early during intestinal T_{RM} cell formation, as previously reported in skin T_{RM} cells[31], these effects did not result in sustained changes in the proportions or absolute numbers of Eomes cKO CD8+ T_{RM} cells, compared to their control counterparts, in any of the four intestinal tissue compartments. Similar results were observed using P14 T cells in which Eomes was inducibly deleted prior to adoptive transfer and LCMV infection, arguing against the possibility of a compensatory adaptation by Eomes cKO CD8+ P14 T cells (Figures S6K and S6L).

We next sought to evaluate the role of Eomes in the maintenance of T_{RM} cells, once established, in each of the four intestinal tissue compartments. Congenically distinct control and *Eomes*$^{fl/fl}$*Cre-ER*^{T2} (Eomes inducible (i)KO) CD8+ P14 T cells were adoptively transferred at a 1:1 ratio into recipient mice subsequently infected with LCMV (Figure 6A). At 21 days post-infection, mice were treated with tamoxifen for 5 days and analyzed after 31 days post-infection. Compared to control cells, the proportions and absolute numbers of Eomes iKO CD8+ P14 T cells were markedly reduced in the siIEL and siLPL compartments, but not in the cIEL and cLPL compartments (Figures 6B and 6C). Eomes iKO P14 T cells exhibited a modest increase in the proportion of cells expressing both CD69 and CD103 (Figure 6D), along with minimal changes in GzmA and GzmB expression (Figures S7A and S7B). The reduction in proportions of Eomes iKO CD8+ P14 T cells in the siIEL and siLPL compartments appeared to affect both CD69+CD103+ and CD69+CD103− subpopulations equally (Figure 6E). In the spleen, the proportions and absolute numbers of total Eomes iKO circulating memory P14 T cells were decreased (Figure 6F), along with a reduced proportion of T_{CM} cells and an increased proportion of t-T_{EM} cells (Figure 6G), suggesting a role for Eomes in the maintenance of established T_{CM} cells in addition to its known role in their formation[45]. Taken together, these findings reveal that Eomes plays a previously unappreciated role in the maintenance of established intestinal CD8+ T_{RM} cells after their formation, with a greater role in the SI than in the colon.

Eomes regulates the maintenance of SI T_{RM} cells, in part, by inducing the anti-apoptotic regulator Bcl-2.

To elucidate potential mechanisms by which Eomes regulates the maintenance of SI T_{RM} cells, we performed CITE-seq on Eomes iKO P14 CD8+ T cells harvested after day 31 post-infection following 5 daily doses of tamoxifen i.p. starting at day 21 post-infection.

Pathway analyses of genes differentially expressed between control and Eomes iKO CD8$^+$ T$_{RM}$ cells from each of the four intestinal tissue compartments revealed an enrichment of genes encoding components of pathways related to apoptosis, cell survival, TGFβ signaling, and cytokine signaling (Table S7). Indeed, transcripts encoding TGFβ signaling components such as *Smad3* were reduced in Eomes iKO intestinal T$_{RM}$ cells compared to control cells, while expression of *Il7r*, the gene encoding for IL-7Rα (CD127), was reduced in Eomes iKO intestinal T$_{RM}$ cells compared to control cells (Figure 7A). Moreover, the anti-apoptotic genes *Bcl2* and *Mcl1* were more highly expressed in control SI T$_{RM}$ cells compared to Eomes iKO cells (Figure 7A; Table S7). At the protein level, Eomes iKO intestinal T$_{RM}$ cells expressed less CD127, both in terms of proportions and on a per-cell basis (Figure S7C). We also examined the levels of the purinergic receptor P2RX7, a sensor of extracellular ATP, in light of its reported role as a key regulator of T$_{RM}$ cell fitness and survival[37,46]. Eomes iKO intestinal T$_{RM}$ cells expressed higher levels of P2RX7 protein (Figure S7D), along with lower levels of Bcl-2 protein (Figure 7B). In line with these observations, forced expression of Eomes resulted in increased expression of Bcl-2 and reduced expression of P2RX7 (Figures 7C, S7E, and S7F). Taken together, these results raised the possibility that Eomes might support SI T$_{RM}$ cell maintenance by virtue of regulating genes and pathways involved in TGFβ signaling, responsiveness to homeostatic cytokines, and/or apoptosis.

We next sought to test whether exogenous administration of IL-7 or shRNA-mediated deletion of P2RX7 might prevent the loss of SI T$_{RM}$ cells resulting from induced deletion of Eomes. Neither administration of IL-7-anti-IL-7 mAb complexes, which substantially increase the *in vivo* biological activity of IL-7[47], nor deletion of P2RX7 ameliorated the reduction of SI T$_{RM}$ cells resulting from the loss of Eomes (Figures S7G–S7J). We therefore asked whether induced deletion of TGFβR2 in established intestinal T$_{RM}$ cells might phenocopy the numerical deficiency of SI T$_{RM}$ cells resulting from the loss of Eomes. Accordingly, congenically distinct control and *Tgfbr2*$^{fl/fl}$*Cre-ER*^{T2} (TGFβR2 inducible (i)KO) CD8$^+$ P14 T cells were adoptively co-transferred at a 1:1 ratio into recipient mice subsequently infected with LCMV (Figure 7D). At 21 days after infection, mice were treated with tamoxifen daily for 5 days and then analyzed after 31 days post-infection. Compared to control cells, the proportions of TGFβR2 iKO CD8$^+$ P14 T cells were reduced only in the siIEL compartment, but not in the other three intestinal tissue compartments (Figure 7E). However, in both the siEL and siLPL compartments, the loss of TGFβR2 led to decreased proportions of CD69$^+$CD103$^+$ T$_{RM}$ cells, but increased proportions of CD69$^+$CD103$^-$ T$_{RM}$ cells (Figures 7F). Thus, CD69$^+$CD103$^+$ and CD69$^+$CD103$^-$ T$_{RM}$ cells in the siIEL and siLPL compartments appeared to be discordantly impacted by the deletion of TGFβR2 (Figure 7G). This experimental finding was distinct from that observed from the loss of Eomes, which reduced both CD69$^+$CD103$^+$ and CD69$^+$CD103$^-$ subpopulations among established Eomes iKO SI T$_{RM}$ cells (Figure 6E). In parallel, we observed that forced TGFβR2 overexpression failed to ameliorate the reduction of SI T$_{RM}$ cells resulting from the loss of Eomes (Figures 7H and 7I). Taken together, these results suggest that while TGFβ signaling plays a critical role in the maintenance of CD69$^+$CD103$^+$ SI T$_{RM}$ cells, the reduction in Eomes iKO SI T$_{RM}$ cells does not appear to be mechanistically linked to alterations in TGFβ signaling.

Lastly, as Eomes iKO intestinal T_{RM} cells expressed lower levels of Bcl-2 (Figure 7B) whereas forced expression of Eomes resulted in increased expression of Bcl-2 (Figure 7C), we asked whether forced expression of Bcl-2 might be capable of preventing the loss of SI T_{RM} cells resulting from the induced deletion of Eomes. Congenically distinct P14 T cells from control and Eomes iKO mice were transduced with empty vector (EV) or Bcl-2 retroviral constructs, mixed at a 1:1 ratio, and adoptively transferred into CD45.2+ recipients prior to infection with LCMV. Mice received 5 daily doses of tamoxifen starting at day 12 post-infection and intestinal tissue compartments were harvested on day 17 post-infection (Figure 7H). Eomes iKO cells transduced with the EV construct exhibited a competitive disadvantage in the SI compared to wild-type cells transduced with the EV construct (Figure 7I), recapitulating the phenotype observed in untransduced cells (Figure 6B, 6C). By contrast, Eomes iKO cells transduced with the Bcl-2 construct were much better able to compete with wild-type cells transduced with the Bcl-2 construct (Figure 7I). In order to distinguish whether the regulation of Bcl-2 by Eomes was direct or indirect, we analyzed our scATAC-seq intestinal T_{RM} cell dataset in conjunction with a previously published Eomes ChIP-seq (chromatin immunoprecipitation sequencing) dataset[32,48]. These analyses revealed accessible regions of chromatin within the *Bcl2* gene locus in intestinal T_{RM} cells that corresponded to putative Eomes binding sites identified by ChIP-seq (Figure 7J). Taken together, these results support the hypothesis that Eomes promotes the survival and maintenance of SI T_{RM} cells, in part, through potentially direct effects on Bcl-2.

DISCUSSION

Emerging data indicate that T_{RM} cells from different tissues exhibit substantial heterogeneity[5,21–23] and an increasing number of studies have highlighted heterogeneity even among T_{RM} cells within the same organ. For example, CD103+ vs. CD103− T_{RM} cells within the brain, salivary gland, and SI exhibit differences in transcriptional profiles[10], developmental plasticity[22], and responsiveness to secondary infection[49,50], respectively. In the siIEL compartment, the IL-2Rα^{lo} CD8+ T cell subpopulation contains putative T_{RM} precursor cells, while the IL-2Rα^{hi} T cell subpopulation may represent a transient, more terminally differentiated subpopulation[51]. Moreover, Blimp1^{hi}Id3^{lo} and Blimp1^{lo}Id3^{hi} cells in the siIEL compartment are prominent at distinct phases of infection and exhibit distinct cytokine capabilities, secondary memory potential, and transcriptional programs[11]. Our data suggest differential requirements for the maintenance of T_{RM} cell subpopulations within the same tissue, as TGFβ signaling was required to promote maintenance of CD103+, but not CD103− T_{RM} cells, within the siIEL and siLPL compartments; by contrast, both CD103+ and CD103− T_{RM} cells from the siIEL and siLPL compartments required Eomes for their continued maintenance.

Our study highlights the emerging concept that factors required for T_{RM} cell formation may be distinct from those required for maintenance after their establishment. Factors that regulate T_{RM} cell formation, but that have not been formally investigated in their maintenance, include Ahr (skin[39]); Blimp1 (skin, kidney, siIEL/siLPL[20], and lung[24]); Hobit (skin, kidney, and siIEL/siLPL[20,32]); Bhlhe40 (lung[52]); Nr4a1 (siIEL, liver[53]), and Nr4a2 (siIEL[51]); and IL-15 signaling (salivary gland, kidney[27], and skin[18]). Factors that play a critical role in both the initial formation and maintenance of T_{RM} cells include Runx3

(siIEL, salivary gland, kidney, lung, skin[11]); TGFβ (skin[18,54], siIEL[18,23], and salivary gland[23]); and P2RX7 (siIEL[37,38,46]). Notably, however, a factor that plays a role in the formation of T_{RM} cells need not be necessary for their maintenance, as previously demonstrated for ICOS in the kidney and siIEL compartment[28]. The data presented here indicate that, like ICOS, Eomes plays distinct roles in the formation vs. maintenance of intestinal T_{RM} cells.

Eomes was first described as a regulator of effector CD8+ T cell responses owing to its effects in directly promoting GzmA expression[55], and was subsequently shown to play an important role in the formation of circulating memory T cells, particularly T_{CM} cells[44,45]. By contrast, T_{RM} cells in the skin, lung, and siIEL compartment were observed to exhibit reduced expression of Eomes compared to circulating memory cells[18]. Moreover, forced expression of Eomes led to reduced T_{RM} cell formation in the skin[31], whereas deletion of endogenous Eomes led to increased T_{RM} cell formation in the liver and kidney[32]. On the basis of these findings, Eomes has been generally regarded as a negative regulator of T_{RM} cell formation, but its role in the maintenance of established T_{RM} cells has not been previously investigated. Our data indicate that Eomes is dispensable for intestinal T_{RM} cell formation, but plays a critical role in the maintenance of established T_{RM} cells in the SI, but not in the colon, in spite of lower baseline expression of Eomes by SI T_{RM} cells. This observation calls into question the seemingly intuitive notion that higher transcription factor expression levels imply greater functional importance. Taken together, these findings suggest that the role of Eomes in T_{RM} cells may more nuanced than previously appreciated, with distinct functions that are dependent on the specific tissue compartment as well as the phase of differentiation.

Lastly, our study adds to the field's understanding of T_{RM} cell plasticity. It was initially thought that T_{RM} cells are terminally differentiated, with limited proliferative capacity after rechallenge and low developmental plasticity. It is now understood that T_{RM} cells are capable of proliferation after reactivation in situ[56,57]; moreover, reactivated T_{RM} cells can leave tissues and egress to the circulation, giving rise to circulating memory T cells[5,6]. Progeny of intravenously transferred ex-siIEL T_{RM} cells maintain a predilection for repopulating the siIEL and siLPL compartments, but not other tissue compartments such as the salivary gland or female reproductive tract[5,9]. Moreover, ex-siIEL T_{RM} cells tend to acquire phenotypic characteristics of their new environment, while retaining some traces of their original tissue of residence[5]. Notably, the developmental plasticity of T_{RM} cells has been reported to differ between some tissues, with ex-liver and ex-siIEL T_{RM} cells exhibiting a greater degree of developmental plasticity than ex-skin T_{RM} cells[21,22]; moreover, CD103− ex-salivary gland T_{RM} cells exhibit a higher degree of developmental plasticity than CD103+ ex-salivary gland T_{RM} cells[22]. Our data suggest that T_{RM} cells located in different anatomic regions of the same organ may also exhibit distinct degrees of developmental plasticity, as ex-siIEL T_{RM} cells were capable of giving rise to secondary T_{RM} cells in all four intestinal tissue compartments and did so to a greater degree than ex-siLPL T_{RM} cells. In addition, we observed that ex-siIEL T_{RM} cells can contribute to the formation of secondary T_{EM} cells in the spleen, but have limited capacity to form secondary T_{CM} cells, in agreement with a prior study[21]. Furthermore, in light of a prior report showing that CD8+ T_{RM} cells can migrate between the siIEL and siLPL compartments[58], our data

raise intriguing questions about the developmental relationships between T_{RM} cells in the siIEL and siLPL compartments during their initial formation. Overall, our study reveals substantial phenotypic, transcriptional, epigenetic, and functional heterogeneity among T_{RM} cells from the four intestinal tissue compartments, and provides a resource for the field to begin to investigate the differential molecular requirements of intestinal T_{RM} cells.

Limitations of the study

In this study, we defined cells as T_{RM} if they were 'i.v.-negative' following i.v. injection of anti-CD8α antibodies into recipient mice 3–5 minutes prior to sacrifice, a widely used approach that labels cells with access to the vasculature during the short pulse prior to sacrifice; it should be noted, however, that this technique does not directly identify T_{RM} cells. Second, T_{RM} cells were analyzed after 21 days post-infection, ~2 weeks after LCMV-Armstrong is cleared in the SI and colon[59–61]; however, it remains possible that antigen may persist in certain anatomical regions and could influence T_{RM} cell differentiation and heterogeneity[62]. Third, although we identified a role for Eomes in the maintenance of established SI T_{RM} cells, technical challenges precluded direct assessment of the consequences of Eomes-deficiency in intestinal T_{RM} cells on host health. Lastly, it should be noted that differences in trafficking, proliferation, and/or survival between ex-siIEL and ex-siLPL T_{RM} cells could contribute to apparent disparities in developmental plasticity.

STAR METHODS

RESOURCE AVAILABILITY

Lead Contact—Further information and requests for the resources and reagents should be directed to and will be fulfilled by the lead contact, John T. Chang (changj@ucsd.edu).

Materials Availability—All the mouse lines used in this study are available from Jackson Laboratories. This study did not generate new unique reagents.

Data and Code Availability—All data reported in this paper are available at Gene Expression Omnibus under accession number GSE205942.

EXPERIMENTAL MODEL AND SUBJECT DETAILS

Mice—All mice were housed under specific pathogen-free conditions in an American Association of Laboratory Animal Care-approved facility at UCSD, and all procedures were approved by the UCSD Institutional Animal Care and Use Committee. C57BL/6J (CD45.2) and B6.SJL-*Ptprc^a^Pepc^b^/BoyJ* (CD45.1) mice were purchased from the Jackson Laboratory. *Tgfbr2*^fl/fl^, *Eomes*^fl/fl^, *Cd4-Cre^+^*, *Ert2-Cre^+^* were purchased from Jackson Laboratory and bred together with P14 TCR transgenic mice to generate *Tgfbr2*^fl/fl^*Ert2-Cre^+^* (TGFβR2 iKO), *Eomes*^fl/fl^*Cd4-Cre^+^* (Eomes cKO) and *Eomes*^fl/fl^*Ert2-Cre^+^* (Eomes iKO) P14 mice. All mice were used at 6–9 weeks of age.

METHOD DETAILS

Adoptive transfer and infection—CD45.1^+^ CD8^+^ P14 T cells were adoptively transferred into CD45.2^+^ recipient mice (1 × 10^5^ cells/mouse). For competition experiments,

TGFβR2 iKO, Eomes cKO, Eomes iKO CD8$^+$ P14 T cells (1 × 10^5 cells/mouse) were co-transferred with control CD8$^+$ P14 T cells (1 × 10^5 cells/mouse). Recipient mice were bled at 21 days post-infection to ensure successful adoptive transfer and to correct for the input ratios between control CD8$^+$ P14 T cells vs. TGFβR2 iKO, Eomes cKO, or Eomes iKO CD8$^+$ P14 T cells. Recipient mice were infected intraperitoneally (i.p.) with 2 × 10^5 plaque-forming units (p.f.u.) of LCMV-Armstrong 30 minutes following adoptive transfer.

Tamoxifen treatment—For inducible deletion of *Eomes* or *Tgfbr2*, tamoxifen was administered i.p. (1 mg/mouse daily × 5 days) at timepoints indicated in the figure legends. A 100 mg/mL tamoxifen stock solution prepared in 100% ethanol was subsequently diluted 1:10 in 100% sunflower seed oil; 100 μL of this was administered for a working dose of 1 mg/mouse/day.

Retroviral transduction—PLAT-E cells (Cell BioLabs) were transfected with empty vector (EV), overexpression vectors (*Eomes, Bcl2, Tgfbr2*), non-targeting shRNA construct, or shRNA constructs targeting *P2rx7* (Transomic) with TransIT-LT1 Reagent (Mirus). The *Eomes* vector was provided by Dr. Steven Reiner, Columbia University; the *Bcl2* vector was provided by Dr. Michael Croft, La Jolla Institute for Immunology; and the *Tgfbr2* vector was provided by Dr. Wanjun Chen, National Institutes of Health. Retroviral supernatants were harvested 48h and 72h post-transfection. CD8$^+$ T cells were isolated using the CD8$^+$ T cell isolation kit (Miltenyi) and activated with plates coated with 100 μg/mL of goat anti-hamster IgG (H+L, Thermo Fisher Scientific), 10 μg/mL of anti-CD3 (3C11, BioXCell), and 10 μg/mL of anti-CD28 (37.51, BioXCell). After 18–22 hours of activation, the cells were 'spinfected' with retroviral supernatant supplemented with 8 g/mL of polybrene (Millipore) at 900g for 90 min at room temperature. The retroviral supernatant was replaced by culture media and the cells were incubated at 37°C. Transduction efficiency was measured based on ametrine or GFP signal using flow cytometry at 24h and 48h post-transduction.

Plasticity experiments—For experiments assessing T$_{RM}$ cell developmental plasticity, CD45.1$^+$ CD8$^+$ P14 T cells were adoptively transferred into congenic CD45.2$^+$ recipients 30 minutes prior to infection with LCMV; siIEL and siLPL T$_{RM}$ cells were FACS-purified from recipient mice more than 21 days following infection, followed by transfer into new, separate CD45.2$^+$ recipients 30 minutes prior to infection with LCMV and euthanized 10–14 days later.

Rescue experiments—Purified CD45.1$^+$ control and CD45.1.2$^+$ Eomes iKO CD8$^+$ P14 T cells were isolated as described above; cells were activated *in vitro* and transduced with empty vector construct, overexpression constructs (*Bcl2, Tgfbr2, P2rx7*), non-targeting shRNA construct, or shRNA constructs targeting *P2rx7* as described above. Retrovirally transduced cells were mixed at a 1:1 ratio and adoptively transferred into congenic recipients, followed by infection with LCMV. Recipient mice were bled at 10 days post-infection to ensure successful adoptive transfer and to correct for the input ratio between control and Eomes iKO CD8$^+$ P14 T cells. For inducible deletion of *Eomes*, tamoxifen was administered i.p. daily × 5 days starting at 12 days post-infection. Recipient mice were euthanized at 17 days post-infection for analysis. For rescue experiments with IL-7-

anti-IL-7 mAb complexes, CD45.1$^+$ control (1×10^5 cells/mouse) and CD45.1.2$^+$ Eomes iKO (1×10^5 cells/mouse) CD8$^+$ P14 T cells were adoptively co-transferred into CD45.2$^+$ recipient mice followed by i.p. infection with LCMV. Recipient mice were bled at 10 days post-infection to ensure successful adoptive transfer and to correct for the input ratio between control and Eomes iKO CD8$^+$ P14 T cells. IL-7/anti-IL-7 mAb complexes were generating by mixing 1.5 μg of recombinant murine IL-7 (Peprotech) with 15 μg of anti-IL-7 mAb (M25, BioXCell), followed by incubation at 30 min at 37°C, as previously described[47]. IL-7/anti-IL-7 mAb complexes and tamoxifen were administered i.p. once daily × 5 days starting at day 12 post-infection. Recipient mice were euthanized at 17 days post-infection for analysis.

Lymphocyte isolation—3–5 minutes prior to sacrifice, mice were injected i.v. with anti-CD8α antibodies to label and exclude cells with access to the circulation. Lymphocyte isolation for spleen and the small intestine and colon IEL compartments was performed as previously reported[51]. To isolate lymphocytes from the small intestine and colon LPL compartment, the remaining tissues were incubated while shaking at 37°C for 15 minutes in IEL solution (1mM EDTA in 1x PBS). The tissues were washed with HBSS then cut thoroughly and resuspended in LPL solution (1640 RPMI, 10% FBS, 100 mg/mL DNase, and 0.02 g/L collagenase IV). Tissues were shaken and incubated at 37°C for 12 minutes. LPL supernatant was collected and filtered into a cell strainer to yield a single-cell suspension. Quantitation of T$_{RM}$ cell numbers reported in Figure 1B were derived by dividing the total number of i.v.-negative CD8 T$_{RM}$ cells quantitated in each intestinal compartment after digestion by the organ weight measured prior to digestion. The purpose of the organ weight normalization was to provide context for the reported numbers. The small intestine was typically larger (~0.7 g) than the colon (~0.2 g); hence, we aimed to show that the increased numbers of T$_{RM}$ cells observed in the small intestine were not simply due to increased size of that organ. Non-normalized absolute numbers are provided as Figure S1A.

Flow cytometry and sorting—For all analyses shown in this study, in order to exclude circulating cells, anti-CD8α antibodies were injected i.v. into recipient mice 3–5 minutes prior to sacrifice and only 'i.v.-negative' cells were considered to be tissue-resident for subsequent downstream analyses; this approach has been widely used to exclude circulating cells with access to the vasculature[34]. Spleen, siIEL, siLPL, cIEL, and cLPL intestinal tissue samples were isolated in a single-cell suspension and stained in Fixable Viability Dye eFluor780 (Thermo Fisher Scientific) at 1:1000 on ice for 10 minutes in the dark. Cells were then surface-stained for 30 minutes on ice with the following antibodies from Biolegend (CD103 (2E7), CD122 (TM-β1), CD127 (A7R34), CD160 (7H1), CCR6 (29-2L17), CCR9 (CW-1.2), CD27 (LG.3A10), CD29 (HMβ1 – 1), CD314 (CX5), CD38 (90), CD44 (IM7), CD45.1 (A20), CD45.2 (104), CD49a (HM1), CD49d (R1-2), CD62L (MEL-14), CD69 (H1.2F3), CD8a (53–6.7), CD8b (TS156.7.7), CXCR3 (CXCR3-173), CXCR4 (L276F12), IL-18R (A17071D), Integrin β7 (FIB27), Ki67 (11F6), KLRG1 (MAFA), Ly6c (HK1.4), P2RX7 (1F11)); or R&D Systems (TGFR2). For experiments involving retrovirally transduced P14 T cells, cells were fixed in 2% paraformaldehyde (Electron Microscopy Services) at room temperature for 20 minutes. For intracellular and intranuclear

staining, cells were fixed and permeabilized using the FoxP3/Transcription Factor Staining Buffer Kit (Thermo Fisher Scientific). For assessment of cytokine production, cells were cultured in the presence of LCMV gp$_{33-41}$ peptide (GenScript) and Protein Transport Inhibitor Cocktail (Thermo Fisher Scientific) for 3h at 37°C, fixed and permeabilized with FoxP3/Transcription Factor Staining Buffer Kit for 30 minutes at room temperature, and then stained with the following antibodies from Biolegend (Bcl-2 (BCL/10C4), GzmB (QA16A02), IFN (XMG1.2), IL-2 (JES6-5H4), T-bet (4B10)); or Thermo Fisher (Eomes (Dan11mag), GzmA (GzA-3G8.5)) at room temperature for 30 minutes.

CITE-seq—Control and Eomes iKO CD8$^+$ P14 T cells were harvested from the siIEL, siLPL, cIEL, and cLPL tissue compartments and spleens from 20 recipient mice infected more than 21 days prior, FACS-purified, and processed through the 10x Genomics pipeline. The single-cell library method used was the Chromium Next GEM Single Cell v3 with single-indexing. The RNA samples and ADT samples were pooled separately. RNA samples were sequenced to a depth of 20,000 reads/cell and ADT (protein) samples were sequenced to a depth of 5,000 reads/cell on a NovaSeq S4.

Single-cell ATAC-seq—CD8$^+$ P14 T cells were harvested from the siIEL, siLPL, cIEL, and cLPL tissue compartments from recipient mice infected more than 21 days prior and purified by FACS. Nuclei were isolated and prepared for single-cell libraries using the Chromium Next GEM Single Cell ATAC Library & Gel Bead Kit v1.1. The pooled libraries of each sample were sequenced on a NovaSeq S4.

QUANTIFICATION AND STATISTICAL ANALYSIS

Flow cytometry—For analysis, all samples were run on a LSRFortessa X-20 (BD Biosciences) or Novocyte 3000 (Agilent). Samples for FACS-purified with an Influx, FACSAria Fusion, or FACSAria2 (BD Biosciences). BD FACS DIVA (BD Biosciences) or NovoExpress (Agilent) software was used for data collection, and FlowJo software (BD Biosciences) was used for analysis of flow cytometry data. In general, when available, a biologic negative control not expressing the marker of interest was used to set gates; if not available, an isotype control or Fluorescence Minus One (FMO) control was used to set gates. A biologic negative control was used for the following antibodies: CCR6, CCR9, CD8β, CD27, CD29, CD38, CD44, CD45.1, CD45.2, CD49a, CD49d, CD62L, CD69, CD103, CD160, CD314, CXCR3, CXCR4, Eomes, GzmA, GzmB, IFNγ, IL-2, IL-18R, integrinβ7, Ki67, KLRG1, Ly108, Ly6C, P2RX7, T-bet, and TNF. An isotype negative control was used for the following antibodies: Bcl-2, CD122, and CD127. An FMO negative control was used for the following antibody: CD8α (i.v. label). Statistical analysis of flow cytometry data was performed using Prism software (GraphPad). P values of <0.05 were considered significant. Statistical details for each experiment are provided in the figure legends.

CITE-seq—The Cell Ranger 6.0.1 pipeline was used to align, filter, and quantify counts using a reference mouse genome file (mm10-3.0.0). The resulting UMI count matrices were read into Seurat 4.1.0.9001, and further filtered based on mitochondrial percentage. Cells with mitochondrial percentage greater than 5% were removed. The metrics from the

Cellranger count pipeline were used to assess sample quality. All samples passed through the pipeline successfully. Sequencing saturation for samples was 88% and above. Valid barcodes and valid UMIs were all above the threshold of 75%, with values greater that 96% and 100% respectively. The fraction reads in cells for all samples were 85% and above, and all samples had reads mapped antisense to gene value of 2% or less, which passed the quality threshold of an ideal sample being less than 10%. There was no threshold for the number of cells collected during the Cellranger count pipeline. All samples had a %Q30 score of greater than 70, % perfect index reads of 85% and above, and raw cluster percentages of less than 7%.

After this pre-processing, cells from each sample were selected to be used for the downstream analysis with data from both the 'Gene Expression' and 'Antibody Capture' output matrices. Using the RNA assay, the Seurat object was log-normalized, scaled using variable features, and PCA-transformed. These steps were repeated on the ADT (antibody-derived tag) assay after removing features CD45.1 and CD45.2. After the removal of these two features, the Seurat object was normalized using centered log-ratio normalization, scaled, and PCA transformed. The command FindMultiModalNeighbors was used to construct the weighted nearest neighbor (WNN) graph, to find neighbors based on the weighted values of the RNA and ADT assays. The command FindClusters was used to identify clusters within the data base on the graph data from the WNN method. Non-linear dimensional reduction techniques tSNE and UMAP were utilized for visualization. Differentially expressed genes were found using command FindMarkers between clusters, tissue, and samples. Other visualization tools from the Seurat package such DoHeatmap, VlnPlot, and FeaturePlot were used to further explore the data. Pathway analyses were performed using Metascape[36]. It should be noted that the observed correlation between mRNA expression and protein abundance was suboptimal, consistent with prior studies[35,63–65]. There are likely to be many reasons for this lack of correlation, including biologic variations in mRNA stability and turnover as well as the technical limitation that only a small fraction of the transcriptome of the cell is captured ('dropouts') with the widely used 10x Genomics scRNA-seq platform. Thus, CITE-seq may not be the optimal approach to investigate mRNA – protein relationships. Ribosome profiling (termed 'Ribo-seq' or 'ART-seq' (active mRNA translation sequencing) based on sequencing of ribosome-protected mRNA fragments aims to identify transcripts undergoing active translation and may lead to better correlations between mRNA expression and protein abundance in future studies.

Single-cell ATAC-seq—Analysis of scATAC-seq data was completed using the Seurat extension Signac (v1.6.0)[66]. Cellranger outputs for each sample were individually imported into R as Seurat objects. The samples were randomly subsampled to 2000 cells per sample before being merged into a single Seurat object. Annotation, quality control, dimensional reduction, and UMAP creation were completed using the standard Signac workflow. Differentially accessible regions (DAR) between tissues were first obtained using the FindMarkers function in Signac. For each DAR, fragment counts per tissue were compiled using the CountsInRegion function and visualized with a heatmap using pheatmap (v1.0.8). The per-cell motif activity score was calculated by running Signac's implementation of

chromVAR. For each motif, differential activity scores between tissues, along with p values, were then determined by using the FindMarkers function on the chromVAR assay. Selected motifs that were differentially active in a single intestinal compartment (siIEL, siLPL, cIEL, cLPL) and their associated p values are shown in Figures S4D–G. A full list of all differentially active motifs (and associated p values) is also provided in Table S5. Selected motifs differentially active in two intestinal compartments and their associated p values are shown in Figures S4H (siIEL and cIEL), S4I (siLPL and cLPL), and S4J (cIEL and cLPL). For a single selected motif, violin plots in the lower right corner of each figure show the activity scores for individual cells from each of the four intestinal compartments. Statistics were not calculated specifically for the violin plots because the selected motifs shown were already identified as having statistically significant differential activity scores in CD8 T_{RM} cells between the intestinal tissue compartments. Overlapping and unique enriched motifs between tissues were identified and visualized using the R package VennDiagram (v1.7.3). Signac's MotifPlot function was used to generated Motif plots.

scVelo—Differentiation trajectories were inferred using scVelo (v0.2.4). The Cellranger output for each sample was converted into .loom files in command line for import into Python using Velocyto (v0.17.17). In Python, the samples were then merged into a single adata object using scVelo. Filtering, normalization, and moment computing for velocity estimation was completed using scVelo's standard preprocessing steps. The samples were then analyzed using the Dynamical Modeling workflow to create velocity and latent time UMAPs.

Supplementary Material

Refer to Web version on PubMed Central for supplementary material.

ACKNOWLEDGMENTS

INCLUSION AND DIVERSITY

One or more of the authors of this paper self-identifies as an underrepresented ethnic minority in their field of research or within their geographical location. One or more of the authors of this paper self-identifies as a gender minority in their field of research. One or more of the authors of this paper self-identifies as a member of the LGBTQIA+ community. One or more of the authors of this paper self-identifies as living with a disability. One or more of the authors of this paper received support from a program designed to increase minority representation in their field of research.

REFERENCES

1. Chang JT, Wherry EJ, and Goldrath AW (2014). Molecular regulation of effector and memory T cell differentiation. Nature immunology 15, 1104–1115. 10.1038/ni.3031. [PubMed: 25396352]

2. Milner JJ, Nguyen H, Omilusik K, Reina-Campos M, Tsai M, Toma C, Delpoux A, Boland BS, Hedrick SM, Chang JT, and Goldrath AW (2020). Delineation of a molecularly distinct terminally differentiated memory CD8 T cell population. Proc Natl Acad Sci U S A 117, 25667–25678. 10.1073/pnas.2008571117. [PubMed: 32978300]

3. Gerlach C, Moseman EA, Loughhead SM, Alvarez D, Zwijnenburg AJ, Waanders L, Garg R, de la Torre JC, and von Andrian UH (2016). The Chemokine Receptor CX3CR1 Defines Three Antigen-Experienced CD8 T Cell Subsets with Distinct Roles in Immune Surveillance and Homeostasis. Immunity 45, 1270–1284. 10.1016/j.immuni.2016.10.018. [PubMed: 27939671]

4. Sallusto F, Lenig D, Forster R, Lipp M, and Lanzavecchia A (1999). Two subsets of memory T lymphocytes with distinct homing potentials and effector functions. Nature 401, 708–712. 10.1038/44385. [PubMed: 10537110]

5. Fonseca R, Beura LK, Quarnstrom CF, Ghoneim HE, Fan Y, Zebley CC, Scott MC, Fares-Frederickson NJ, Wijeyesinghe S, Thompson EA, et al. (2020). Developmental plasticity allows outside-in immune responses by resident memory T cells. Nature immunology 21, 412–421. 10.1038/s41590-020-0607-7. [PubMed: 32066954]

6. Stolley JM, Johnston TS, Soerens AG, Beura LK, Rosato PC, Joag V, Wijeyesinghe SP, Langlois RA, Osum KC, Mitchell JS, and Masopust D (2020). Retrograde migration supplies resident memory T cells to lung-draining LN after influenza infection. J Exp Med 217. 10.1084/jem.20192197.

7. Gebhardt T, Wakim LM, Eidsmo L, Reading PC, Heath WR, and Carbone FR (2009). Memory T cells in nonlymphoid tissue that provide enhanced local immunity during infection with herpes simplex virus. Nature immunology 10, 524–530. 10.1038/ni.1718. [PubMed: 19305395]

8. Masopust D, Choo D, Vezys V, Wherry EJ, Duraiswamy J, Akondy R, Wang J, Casey KA, Barber DL, Kawamura KS, et al. (2010). Dynamic T cell migration program provides resident memory within intestinal epithelium. J Exp Med 207, 553–564. 10.1084/jem.20090858. [PubMed: 20156972]

9. Masopust D, Vezys V, Wherry EJ, Barber DL, and Ahmed R (2006). Cutting edge: gut microenvironment promotes differentiation of a unique memory CD8 T cell population. J Immunol 176, 2079–2083. 10.4049/jimmunol.176.4.2079. [PubMed: 16455963]

10. Wakim LM, Woodward-Davis A, Liu R, Hu Y, Villadangos J, Smyth G, and Bevan MJ (2012). The molecular signature of tissue resident memory CD8 T cells isolated from the brain. J Immunol 189, 3462–3471. 10.4049/jimmunol.1201305. [PubMed: 22922816]

11. Milner JJ, Toma C, Yu B, Zhang K, Omilusik K, Phan AT, Wang D, Getzler AJ, Nguyen T, Crotty S, et al. (2017). Runx3 programs CD8(+) T cell residency in non-lymphoid tissues and tumours. Nature 552, 253–257. 10.1038/nature24993. [PubMed: 29211713]

12. Park SL, Buzzai A, Rautela J, Hor JL, Hochheiser K, Effern M, McBain N, Wagner T, Edwards J, McConville R, et al. (2019). Tissue-resident memory CD8(+) T cells promote melanoma-immune equilibrium in skin. Nature 565, 366–371. 10.1038/s41586-018-0812-9. [PubMed: 30598548]

13. Savas P, Virassamy B, Ye C, Salim A, Mintoff CP, Caramia F, Salgado R, Byrne DJ, Teo ZL, Dushyanthen S, et al. (2018). Single-cell profiling of breast cancer T cells reveals a tissue-resident memory subset associated with improved prognosis. Nat Med 24, 986–993. 10.1038/s41591-018-0078-7. [PubMed: 29942092]

14. Boland BS, He Z, Tsai MS, Olvera JG, Omilusik KD, Duong HG, Kim ES, Limary AE, Jin W, Milner JJ, et al. (2020). Heterogeneity and clonal relationships of adaptive immune cells in ulcerative colitis revealed by single-cell analyses. Sci Immunol 5. 10.1126/sciimmunol.abb4432.

15. Boyman O, Hefti HP, Conrad C, Nickoloff BJ, Suter M, and Nestle FO (2004). Spontaneous development of psoriasis in a new animal model shows an essential role for resident T cells and tumor necrosis factor-alpha. J Exp Med 199, 731–736. 10.1084/jem.20031482. [PubMed: 14981113]

16. Cheuk S, Schlums H, Gallais Serezal I, Martini E, Chiang SC, Marquardt N, Gibbs A, Detlofsson E, Introini A, Forkel M, et al. (2017). CD49a Expression Defines Tissue-Resident CD8(+) T Cells Poised for Cytotoxic Function in Human Skin. Immunity 46, 287–300. 10.1016/j.immuni.2017.01.009. [PubMed: 28214226]

17. Chang JT (2020). Pathophysiology of Inflammatory Bowel Diseases. N Engl J Med 383, 2652–2664. 10.1056/NEJMra2002697. [PubMed: 33382932]

18. Mackay LK, Rahimpour A, Ma JZ, Collins N, Stock AT, Hafon ML, Vega-Ramos J, Lauzurica P, Mueller SN, Stefanovic T, et al. (2013). The developmental pathway for CD103(+)CD8+ tissue-resident memory T cells of skin. Nature immunology 14, 1294–1301. 10.1038/ni.2744. [PubMed: 24162776]

19. Skon CN, Lee JY, Anderson KG, Masopust D, Hogquist KA, and Jameson SC (2013). Transcriptional downregulation of S1pr1 is required for the establishment of resident memory CD8+ T cells. Nature immunology 14, 1285–1293. 10.1038/ni.2745. [PubMed: 24162775]

20. Mackay LK, Minnich M, Kragten NA, Liao Y, Nota B, Seillet C, Zaid A, Man K, Preston S, Freestone D, et al. (2016). Hobit and Blimp1 instruct a universal transcriptional program of tissue residency in lymphocytes. Science 352, 459–463. 10.1126/science.aad2035. [PubMed: 27102484]

21. Behr FM, Parga-Vidal L, Kragten NAM, van Dam TJP, Wesselink TH, Sheridan BS, Arens R, van Lier RAW, Stark R, and van Gisbergen K (2020). Tissue-resident memory CD8(+) T cells shape local and systemic secondary T cell responses. Nature immunology 21, 1070–1081. 10.1038/s41590-020-0723-4. [PubMed: 32661361]

22. Christo SN, Evrard M, Park SL, Gandolfo LC, Burn TN, Fonseca R, Newman DM, Alexandre YO, Collins N, Zamudio NM, et al. (2021). Discrete tissue microenvironments instruct diversity in resident memory T cell function and plasticity. Nature immunology 22, 1140–1151. 10.1038/s41590-021-01004-1. [PubMed: 34426691]

23. Crowl JT, Heeg M, Ferry A, Milner JJ, Omilusik KD, Toma C, He Z, Chang JT, and Goldrath AW (2022). Tissue-resident memory CD8(+) T cells possess unique transcriptional, epigenetic and functional adaptations to different tissue environments. Nature immunology 23, 1121–1131. 10.1038/s41590-022-01229-8. [PubMed: 35761084]

24. Behr FM, Kragten NAM, Wesselink TH, Nota B, van Lier RAW, Amsen D, Stark R, Hombrink P, and van Gisbergen K (2019). Blimp-1 Rather Than Hobit Drives the Formation of Tissue-Resident Memory CD8(+) T Cells in the Lungs. Front Immunol 10, 400. 10.3389/fimmu.2019.00400. [PubMed: 30899267]

25. Herndler-Brandstetter D, Ishigame H, Shinnakasu R, Plajer V, Stecher C, Zhao J, Lietzenmayer M, Kroehling L, Takumi A, Kometani K, et al. (2018). KLRG1(+) Effector CD8(+) T Cells Lose KLRG1, Differentiate into All Memory T Cell Lineages, and Convey Enhanced Protective Immunity. Immunity 48, 716–729 e718. 10.1016/j.immuni.2018.03.015. [PubMed: 29625895]

26. Holz LE, Prier JE, Freestone D, Steiner TM, English K, Johnson DN, Mollard V, Cozijnsen A, Davey GM, Godfrey DI, et al. (2018). CD8(+) T Cell Activation Leads to Constitutive Formation of Liver Tissue-Resident Memory T Cells that Seed a Large and Flexible Niche in the Liver. Cell Rep 25, 68–79 e64. 10.1016/j.celrep.2018.08.094. [PubMed: 30282039]

27. Schenkel JM, Fraser KA, Casey KA, Beura LK, Pauken KE, Vezys V, and Masopust D (2016). IL-15-Independent Maintenance of Tissue-Resident and Boosted Effector Memory CD8 T Cells. J Immunol 196, 3920–3926. 10.4049/jimmunol.1502337. [PubMed: 27001957]

28. Peng C, Huggins MA, Wanhainen KM, Knutson TP, Lu H, Georgiev H, Mittelsteadt KL, Jarjour NN, Wang H, Hogquist KA, et al. (2022). Engagement of the costimulatory molecule ICOS in tissues promotes establishment of CD8(+) tissue-resident memory T cells. Immunity 55, 98–114 e115. 10.1016/j.immuni.2021.11.017. [PubMed: 34932944]

29. Sheridan BS, Pham QM, Lee YT, Cauley LS, Puddington L, and Lefrancois L (2014). Oral infection drives a distinct population of intestinal resident memory CD8(+) T cells with enhanced protective function. Immunity 40, 747–757. 10.1016/j.immuni.2014.03.007. [PubMed: 24792910]

30. Zhang N, and Bevan MJ (2013). Transforming growth factor-beta signaling controls the formation and maintenance of gut-resident memory T cells by regulating migration and retention. Immunity 39, 687–696. 10.1016/j.immuni.2013.08.019. [PubMed: 24076049]

31. Mackay LK, Wynne-Jones E, Freestone D, Pellicci DG, Mielke LA, Newman DM, Braun A, Masson F, Kallies A, Belz GT, and Carbone FR (2015). T-box Transcription Factors Combine with the Cytokines TGF-beta and IL-15 to Control Tissue-Resident Memory T Cell Fate. Immunity 43, 1101–1111. 10.1016/j.immuni.2015.11.008. [PubMed: 26682984]

32. Parga-Vidal L, Behr FM, Kragten NAM, Nota B, Wesselink TH, Kavazovic I, Covill LE, Schuller MBP, Bryceson YT, Wensveen FM, et al. (2021). Hobit identifies tissue-resident memory T cell precursors that are regulated by Eomes. Sci Immunol 6. 10.1126/sciimmunol.abg3533.

33. Steinert EM, Schenkel JM, Fraser KA, Beura LK, Manlove LS, Igyarto BZ, Southern PJ, and Masopust D (2015). Quantifying Memory CD8 T Cells Reveals Regionalization of Immunosurveillance. Cell 161, 737–749. 10.1016/j.cell.2015.03.031. [PubMed: 25957682]

34. Anderson KG, Sung H, Skon CN, Lefrancois L, Deisinger A, Vezys V, and Masopust D (2012). Cutting edge: intravascular staining redefines lung CD8 T cell responses. J Immunol 189, 2702–2706. 10.4049/jimmunol.1201682. [PubMed: 22896631]

35. Stoeckius M, Hafemeister C, Stephenson W, Houck-Loomis B, Chattopadhyay PK, Swerdlow H, Satija R, and Smibert P (2017). Simultaneous epitope and transcriptome measurement in single cells. Nat Methods 14, 865–868. 10.1038/nmeth.4380. [PubMed: 28759029]

36. Zhou Y, Zhou B, Pache L, Chang M, Khodabakhshi AH, Tanaseichuk O, Benner C, and Chanda SK (2019). Metascape provides a biologist-oriented resource for the analysis of systems-level datasets. Nat Commun 10, 1523. 10.1038/s41467-019-09234-6. [PubMed: 30944313]

37. Borges da Silva H, Beura LK, Wang H, Hanse EA, Gore R, Scott MC, Walsh DA, Block KE, Fonseca R, Yan Y, et al. (2018). The purinergic receptor P2RX7 directs metabolic fitness of long-lived memory CD8(+) T cells. Nature 559, 264–268. 10.1038/s41586-018-0282-0. [PubMed: 29973721]

38. Stark R, Wesselink TH, Behr FM, Kragten NAM, Arens R, Koch-Nolte F, van Gisbergen K, and van Lier RAW (2018). T RM maintenance is regulated by tissue damage via P2RX7. Sci Immunol 3. 10.1126/sciimmunol.aau1022.

39. Zaid A, Mackay LK, Rahimpour A, Braun A, Veldhoen M, Carbone FR, Manton JH, Heath WR, and Mueller SN (2014). Persistence of skin-resident memory T cells within an epidermal niche. Proc Natl Acad Sci U S A 111, 5307–5312. 10.1073/pnas.1322292111. [PubMed: 24706879]

40. Jeannet G, Boudousquie C, Gardiol N, Kang J, Huelsken J, and Held W (2010). Essential role of the Wnt pathway effector Tcf-1 for the establishment of functional CD8 T cell memory. Proc Natl Acad Sci U S A 107, 9777–9782. 10.1073/pnas.0914127107. [PubMed: 20457902]

41. Zhao DM, Yu S, Zhou X, Haring JS, Held W, Badovinac VP, Harty JT, and Xue HH (2010). Constitutive activation of Wnt signaling favors generation of memory CD8 T cells. J Immunol 184, 1191–1199. 10.4049/jimmunol.0901199. [PubMed: 20026746]

42. Bergen V, Lange M, Peidli S, Wolf FA, and Theis FJ (2020). Generalizing RNA velocity to transient cell states through dynamical modeling. Nat Biotechnol 38, 1408–1414. 10.1038/s41587-020-0591-3. [PubMed: 32747759]

43. La Manno G, Soldatov R, Zeisel A, Braun E, Hochgerner H, Petukhov V, Lidschreiber K, Kastriti ME, Lonnerberg P, Furlan A, et al. (2018). RNA velocity of single cells. Nature 560, 494–498. 10.1038/s41586-018-0414-6. [PubMed: 30089906]

44. Intlekofer AM, Takemoto N, Wherry EJ, Longworth SA, Northrup JT, Palanivel VR, Mullen AC, Gasink CR, Kaech SM, Miller JD, et al. (2005). Effector and memory CD8+ T cell fate coupled by T-bet and eomesodermin. Nature immunology 6, 1236–1244. 10.1038/ni1268. [PubMed: 16273099]

45. Banerjee A, Gordon SM, Intlekofer AM, Paley MA, Mooney EC, Lindsten T, Wherry EJ, and Reiner SL (2010). Cutting edge: The transcription factor eomesodermin enables CD8+ T cells to compete for the memory cell niche. J Immunol 185, 4988–4992. 10.4049/jimmunol.1002042. [PubMed: 20935204]

46. Borges da Silva H, Peng C, Wang H, Wanhainen KM, Ma C, Lopez S, Khoruts A, Zhang N, and Jameson SC (2020). Sensing of ATP via the Purinergic Receptor P2RX7 Promotes CD8(+) Trm Cell Generation by Enhancing Their Sensitivity to the Cytokine TGF-beta. Immunity 53, 158–171 e156. 10.1016/j.immuni.2020.06.010. [PubMed: 32640257]

47. Boyman O, Ramsey C, Kim DM, Sprent J, and Surh CD (2008). IL-7/anti-IL-7 mAb complexes restore T cell development and induce homeostatic T Cell expansion without lymphopenia. J Immunol 180, 7265–7275. 10.4049/jimmunol.180.11.7265. [PubMed: 18490726]

48. Kavazovic I, Han H, Balzaretti G, Slinger E, Lemmermann NAW, Ten Brinke A, Merkler D, Koster J, Bryceson YT, de Vries N, et al. (2020). Eomes broadens the scope of CD8 T-cell memory by inhibiting apoptosis in cells of low affinity. PLoS Biol 18, e3000648. 10.1371/journal.pbio.3000648. [PubMed: 32182234]

49. Fung HY, Teryek M, Lemenze AD, and Bergsbaken T (2022). CD103 fate mapping reveals that intestinal CD103(−) tissue-resident memory T cells are the primary responders to secondary infection. Sci Immunol 7, eabl9925. 10.1126/sciimmunol.abl9925. [PubMed: 36332012]

50. von Hoesslin M, Kuhlmann M, de Almeida GP, Kanev K, Wurmser C, Gerullis AK, Roelli P, Berner J, and Zehn D (2022). Secondary infections rejuvenate the intestinal CD103(+) tissue-resident memory T cell pool. Sci Immunol 7, eabp9553. 10.1126/sciimmunol.abp9553. [PubMed: 36332011]

51. Kurd NS, He Z, Louis TL, Milner JJ, Omilusik KD, Jin W, Tsai MS, Widjaja CE, Kanbar JN, Olvera JG, et al. (2020). Early precursors and molecular determinants of tissue-resident memory CD8(+) T lymphocytes revealed by single-cell RNA sequencing. Sci Immunol 5. 10.1126/sciimmunol.aaz6894.

52. Li C, Zhu B, Son YM, Wang Z, Jiang L, Xiang M, Ye Z, Beckermann KE, Wu Y, Jenkins JW, et al. (2019). The Transcription Factor Bhlhe40 Programs Mitochondrial Regulation of Resident CD8(+) T Cell Fitness and Functionality. Immunity 51, 491–507 e497. 10.1016/j.immuni.2019.08.013. [PubMed: 31533057]

53. Boddupalli CS, Nair S, Gray SM, Nowyhed HN, Verma R, Gibson JA, Abraham C, Narayan D, Vasquez J, Hedrick CC, et al. (2016). ABC transporters and NR4A1 identify a quiescent subset of tissue-resident memory T cells. J Clin Invest 126, 3905–3916. 10.1172/JCI85329. [PubMed: 27617863]

54. Hirai T, Yang Y, Zenke Y, Li H, Chaudhri VK, De La Cruz Diaz JS, Zhou PY, Nguyen BA, Bartholin L, Workman CJ, et al. (2021). Competition for Active TGFbeta Cytokine Allows for Selective Retention of Antigen-Specific Tissue- Resident Memory T Cells in the Epidermal Niche. Immunity 54, 84–98 e85. 10.1016/j.immuni.2020.10.022. [PubMed: 33212014]

55. Pearce EL, Mullen AC, Martins GA, Krawczyk CM, Hutchins AS, Zediak VP, Banica M, DiCioccio CB, Gross DA, Mao CA, et al. (2003). Control of effector CD8+ T cell function by the transcription factor Eomesodermin. Science 302, 1041–1043. 10.1126/science.1090148. [PubMed: 14605368]

56. Beura LK, Mitchell JS, Thompson EA, Schenkel JM, Mohammed J, Wijeyesinghe S, Fonseca R, Burbach BJ, Hickman HD, Vezys V, et al. (2018). Intravital mucosal imaging of CD8(+) resident memory T cells shows tissue-autonomous recall responses that amplify secondary memory. Nature immunology 19, 173–182. 10.1038/s41590-017-0029-3. [PubMed: 29311694]

57. Park SL, Zaid A, Hor JL, Christo SN, Prier JE, Davies B, Alexandre YO, Gregory JL, Russell TA, Gebhardt T, et al. (2018). Local proliferation maintains a stable pool of tissue-resident memory T cells after antiviral recall responses. Nature immunology 19, 183–191. 10.1038/s41590-017-0027-5. [PubMed: 29311695]

58. Thompson EA, Mitchell JS, Beura LK, Torres DJ, Mrass P, Pierson MJ, Cannon JL, Masopust D, Fife BT, and Vezys V (2019). Interstitial Migration of CD8alphabeta T Cells in the Small Intestine Is Dynamic and Is Dictated by Environmental Cues. Cell Rep 26, 2859–2867 e2854. 10.1016/j.celrep.2019.02.034. [PubMed: 30865878]

59. Beura LK, Anderson KG, Schenkel JM, Locquiao JJ, Fraser KA, Vezys V, Pepper M, and Masopust D (2015). Lymphocytic choriomeningitis virus persistence promotes effector-like memory differentiation and enhances mucosal T cell distribution. J Leukoc Biol 97, 217–225. 10.1189/jlb.1HI0314-154R. [PubMed: 25395301]

60. Labarta-Bajo L, Nilsen SP, Humphrey G, Schwartz T, Sanders K, Swafford A, Knight R, Turner JR, and Zuniga EI (2020). Type I IFNs and CD8 T cells increase intestinal barrier permeability after chronic viral infection. J Exp Med 217. 10.1084/jem.20192276.

61. Macleod BL, Elsaesser HJ, Snell LM, Dickson RJ, Guo M, Hezaveh K, Xu W, Kothari A, McGaha TL, Guidos CJ, and Brooks DG (2020). A network of immune and microbial modifications underlies viral persistence in the gastrointestinal tract. J Exp Med 217. 10.1084/jem.20191473.

62. Khan TN, Mooster JL, Kilgore AM, Osborn JF, and Nolz JC (2016). Local antigen in nonlymphoid tissue promotes resident memory CD8+ T cell formation during viral infection. J Exp Med 213, 951–966. 10.1084/jem.20151855. [PubMed: 27217536]

63. Maier T, Guell M, and Serrano L (2009). Correlation of mRNA and protein in complex biological samples. FEBS Lett 583, 3966–3973. 10.1016/j.febslet.2009.10.036. [PubMed: 19850042]

64. Myers SA, Rhoads A, Cocco AR, Peckner R, Haber AL, Schweitzer LD, Krug K, Mani DR, Clauser KR, Rozenblatt-Rosen O, et al. (2019). Streamlined Protocol for Deep Proteomic Profiling of FAC-sorted Cells and Its Application to Freshly Isolated Murine Immune Cells. Mol Cell Proteomics 18, 995–1009. 10.1074/mcp.RA118.001259. [PubMed: 30792265]

65. Reimegard J, Tarbier M, Danielsson M, Schuster J, Baskaran S, Panagiotou S, Dahl N, Friedlander MR, and Gallant CJ (2021). A combined approach for single-cell mRNA and intracellular protein expression analysis. Commun Biol 4, 624. 10.1038/s42003-021-02142-w. [PubMed: 34035432]

66. Stuart T, Srivastava A, Madad S, Lareau CA, and Satija R (2021). Single-cell chromatin state analysis with Signac. Nat Methods 18, 1333–1341. 10.1038/s41592-021-01282-5. [PubMed: 34725479]

HIGHLIGHTS

- Small intestine (SI) and colon CD8$^+$ T_{RM} cells are molecularly and functionally distinct

- Anatomically distinct SI T_{RM} cells exhibit disparate degrees of developmental plasticity

- Eomes supports maintenance of established T_{RM} cells in the SI, but not in the colon

- Eomes promotes expression of the anti-apoptotic regulator Bcl-2

Author Manuscript
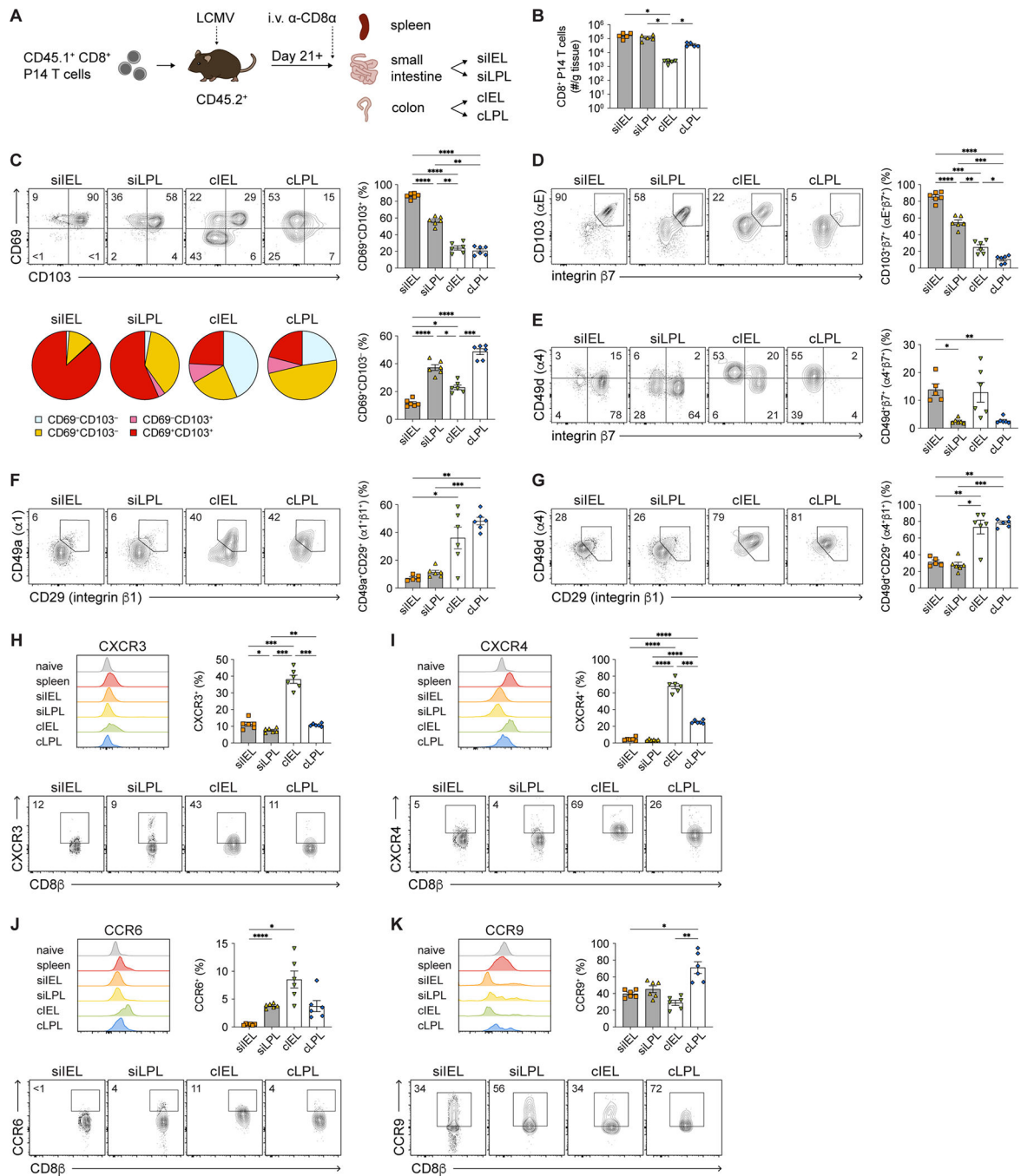
Figure 1. CD8+ T_RM cells in SI and colon express distinct levels of CD69 and CD103.

(A) Experimental design. Spleen and intestinal tissue compartments were isolated from CD45.2+ recipient mice 21 days after LCMV infection following adoptive transfer of donor CD8+CD45.1+ P14 T cells.

(B) Numbers of i.v.⁻ intestinal P14 T cells, normalized to organ weights.

(C) Representative flow cytometry plots showing CD69 and CD103 expression (top left) by i.v.⁻ intestinal P14 T cells. Frequencies (right) of intestinal CD69+CD103+ and

CD69$^+$CD103$^-$ P14 T cells. Distribution of intestinal P14 T cells expressing CD69 and/or CD103 (bottom left).

(D–G) Representative flow cytometry plots showing expression of CD103/integrin β7 (D), CD49d/integrin β7 (E), CD49a/CD29 (F), CD49d/CD29 (G) among i.v.$^-$ intestinal P14 T cells (left). Quantification of indicated integrin heterodimer expression among P14 T cells (right).

(H–K) Representative flow cytometry plots (bottom) showing expression of CXCR3 (H), CXCR4 (I), CCR6 (J), and CCR9 (K) among i.v.$^-$ intestinal P14 T cells. Frequencies of cells expressing each molecule (top right) and representative histograms (top left) indicating the distribution of expression for each molecule; expression by naïve (CD62L^{hi}CD44^{lo}) CD8$^+$ T cells from a separate uninfected mouse is shown for comparison. Data are represented as mean ± SEM. Repeated measures one-way ANOVA. *p<0.05, **p<0.01, ***p<0.001 ****p<0.0001.

Data are representative of ≥3 independent experiments with n=5–6 mice per experiment. See also Figure S1.

Figure 2. Small intestine IEL CD8$^+$ T$_{RM}$ cells express high levels of granzymes whereas cIEL T$_{RM}$ cells exhibit high potential for cytokine production.

(A–E) Histograms (top left), bar graphs (top right), and representative flow cytometry plots (bottom) showing expression of GzmA (A), GzmB (B), IL-2 (C), TNF (D), and IFNγ (E) by i.v.– intestinal P14 T cells.

(F) Proportions of intestinal T cells expressing 0, 1, 2, or 3 cytokines.

(G) Relative change in numbers of intestinal P14 T cells between days 21 and 80 post-infection, normalized to T$_{CM}$ cells.

(H–J) Histograms (top left), bar graphs (top right), and representative flow cytometry plots (bottom) showing expression of CD127 (H), CD122 (I), and CD27 (J) by intestinal P14 T cells.

Data are represented as mean ± SEM. Repeated measures one-way ANOVA. *p<0.05, **p<0.01, ***p<0.001 ****p<0.0001. Data are representative of 3 independent experiments with n=5–6 mice per experiment.

See also Figure S1.
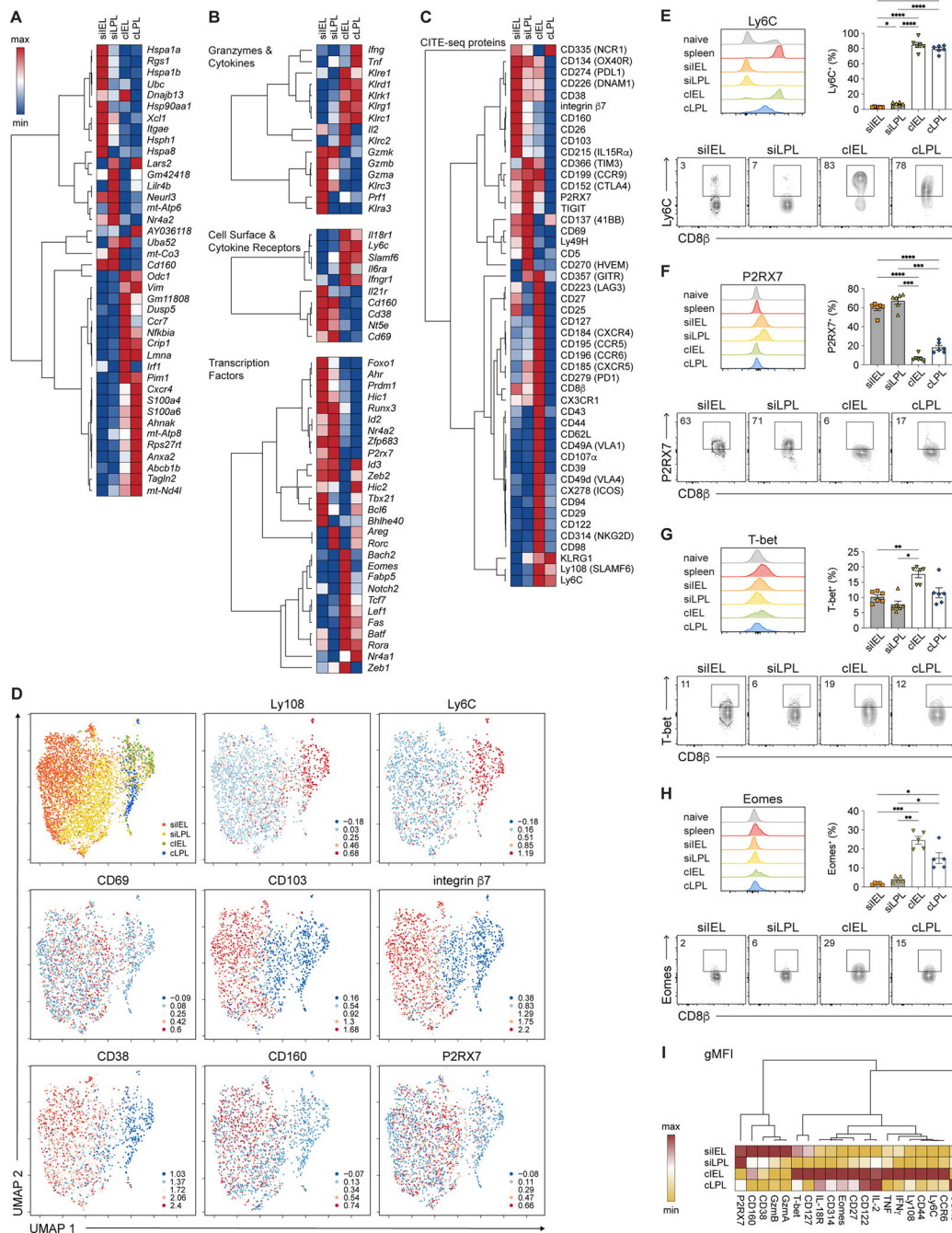
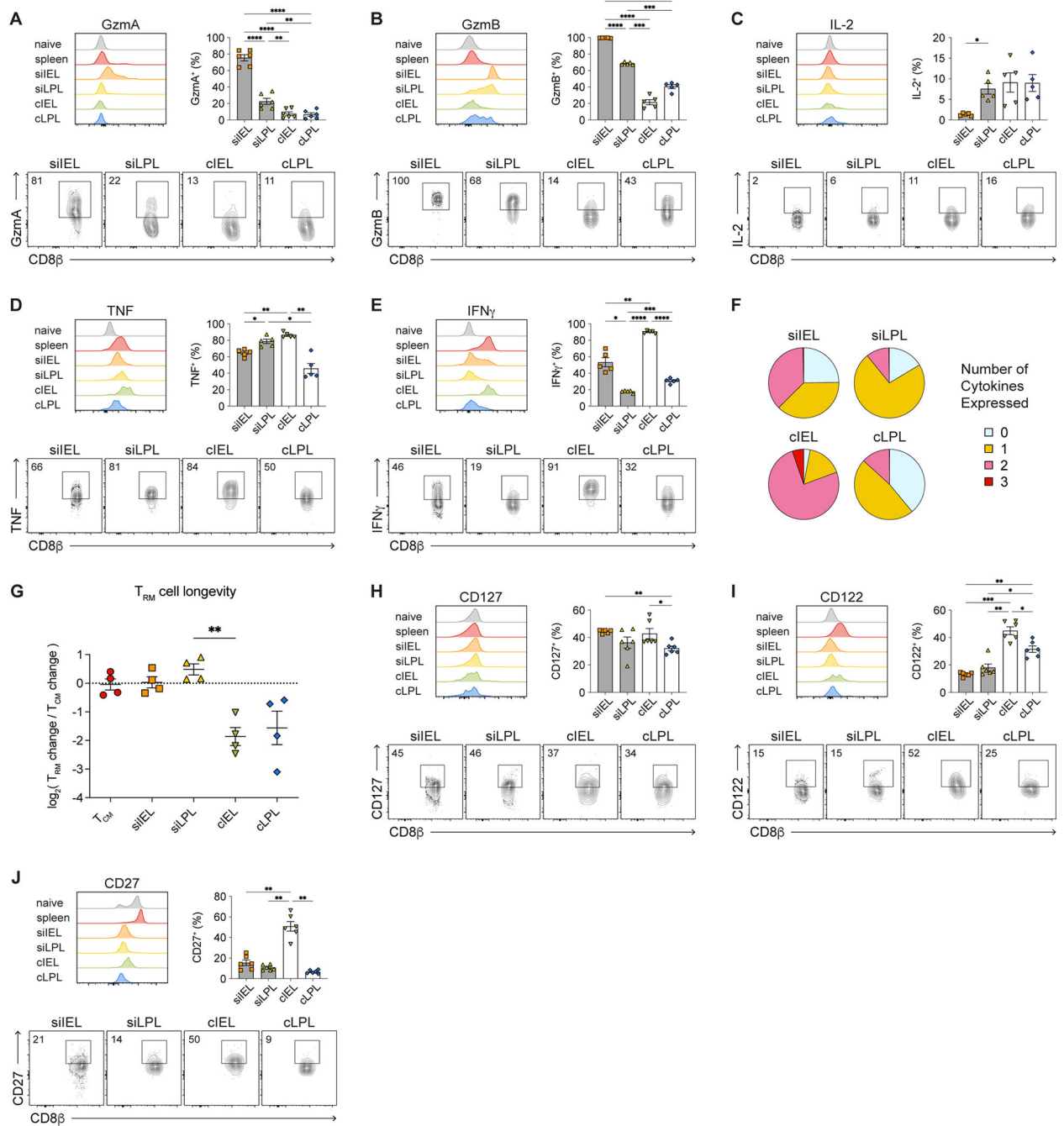**Figure 3. Colon CD8$^+$ T$_{RM}$ cells express higher levels of Eomes than SI T$_{RM}$ cells.**
(A-C) Hierarchically clustered summary heatmaps, derived from CITE-seq data, representing top ten genes differentially expressed among intestinal T$_{RM}$ cells (A); relative expression of selected genes, divided by category (B); or relative expression of all proteins included in the CITE-seq antibody panel (C). Rows represent scaled expression of individual genes (A, B) or proteins (C); columns represent T$_{RM}$ cells from each of the 4 intestinal tissue compartments. Values are mapped to colors using the minimum and maximum of each row.

(D) UMAP plots colored by tissue compartment (top left) or expression of selected proteins superimposed onto individual cells.

(E–H) Histograms (top left), bar graphs (top right), and representative flow cytometry plots (bottom) showing expression of Ly6C (E), P2RX7 (F), T-bet (G), and Eomes (H) among intestinal P14 T cells.

(I) Geometric mean fluorescence intensity (gMFI) of expression of selected proteins by intestinal T_{RM} cells, derived from flow cytometry analyses from Figures 2A–2E, 2H–2J, 3E–3H, and S3C–H, represented as a summary heatmap. Values are mapped to colors using the minimum and maximum of each row.

Data are represented as mean ± SEM. Repeated measures one-way ANOVA. *p<0.05, **p<0.01, ***p<0.001 ****p<0.0001. Data are representative of 3 independent experiments with n=5–6 mice per experiment.

See also Figures S2–S4 and Table S3.
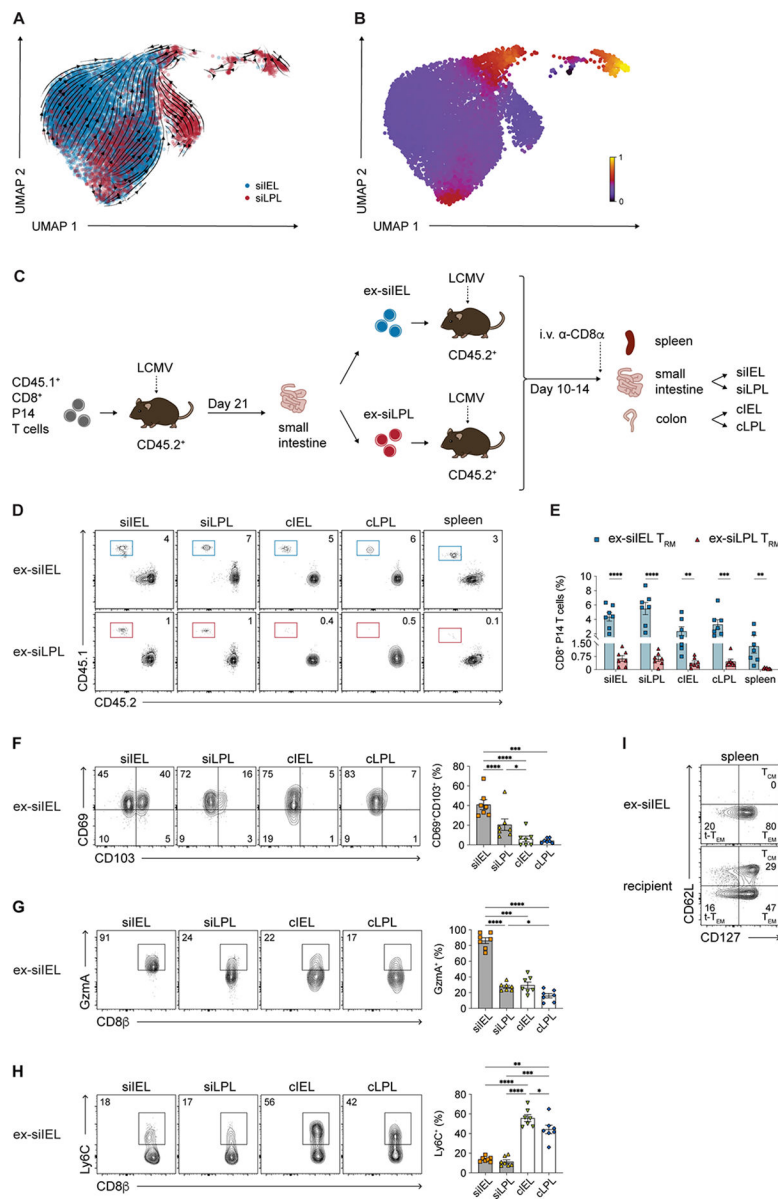
Figure 4. Small intestine IEL T$_{RM}$ cells may exhibit higher developmental plasticity than siLPL T$_{RM}$ cells.

(A and B) Velocities (A) and latent time (B) of siIEL and siLPL T$_{RM}$ cells derived from scVelo projected onto a UMAP-based embedding.

(C) Experimental design. siIEL and siLPL T$_{RM}$ cells were FACS-purified from CD45.2$^+$ recipient mice 21 days following adoptive transfer of donor CD45.1$^+$ P14 T cells and LCMV infection. Cells were transferred into new, separate CD45.2$^+$ recipients subsequently infected with LCMV and sacrificed 10–14 days later.

(D and E) Representative flow cytometry plots (D) and bar graphs (E) showing frequencies of transferred CD45.1$^+$ ex-siIEL (left) or CD45.1$^+$ ex-siLPL (right) T$_{RM}$ cells in the intestinal tissue compartments and spleen.

(F–H) Representative flow cytometry plots (left) and bar graphs (right) showing frequencies of cells expressing CD69 and CD103 (F), GzmA (G), or Ly6C (H) among ex-siIEL T_{RM} cells in the intestinal tissue compartments.

(I) Representative flow cytometry plots showing expression of CD62L and CD127 among ex-siIEL CD8$^+$CD45.1$^+$ P14 T cells or recipient (non-P14) CD8$^+$CD45.2$^+$ T cells in the spleen.

Data are represented as mean ± SEM. Repeated measures one-way ANOVA. *p<0.05, **p<0.01, ***p<0.001 ****p<0.0001. Data are representative of 2 independent experiments with n=5–6 mice per experiment.
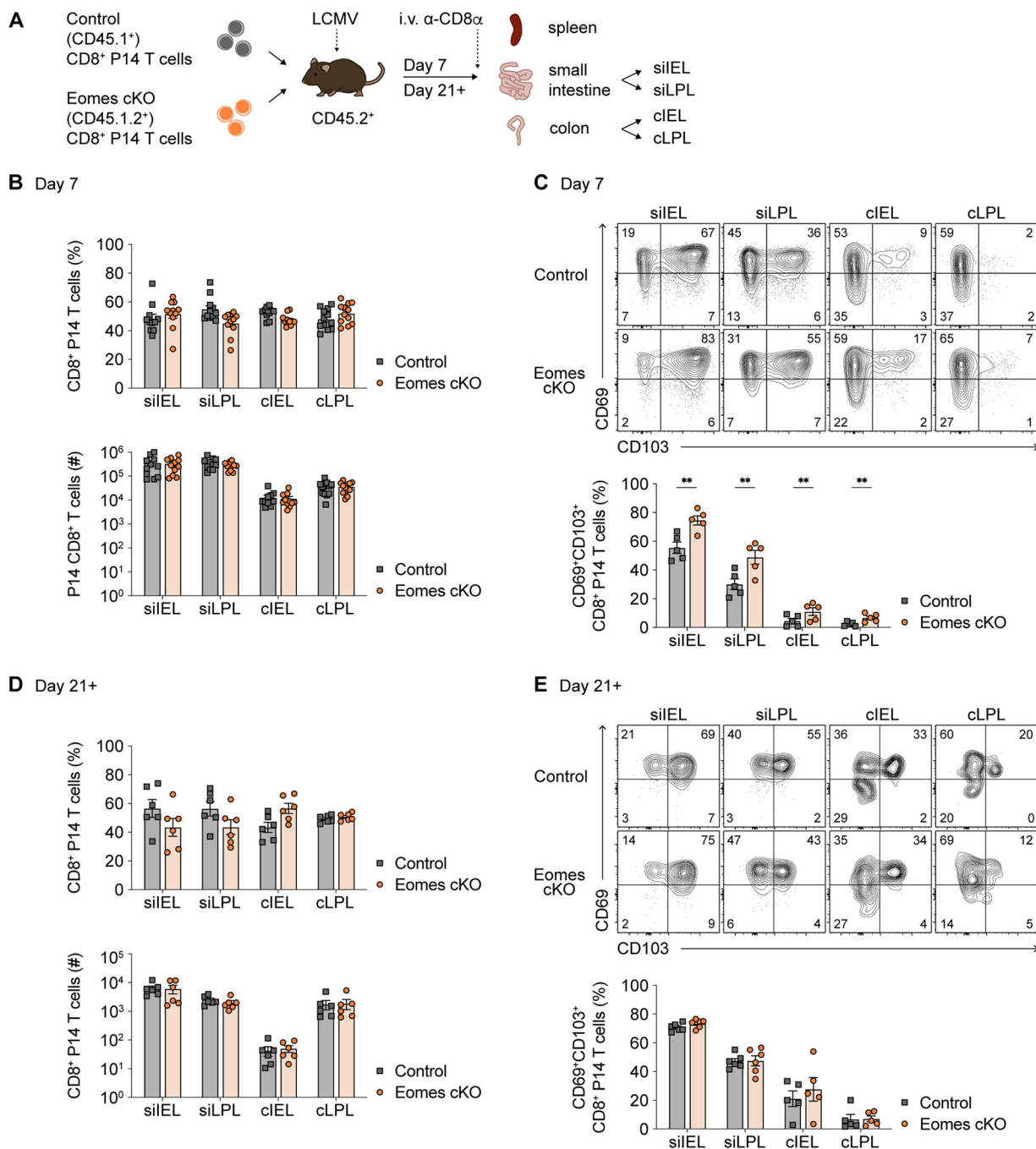
Figure 5. Eomes is dispensable for intestinal CD8$^+$ T$_{RM}$ cell formation.
(A) Experimental design. CD8$^+$ P14 T cells from congenic control and *Eomes*$^{fl/fl}$*Cd4-Cre*$^+$
(Eomes cKO) mice were adoptively co-transferred at a 1:1 ratio into recipients subsequently
infected with LCMV. Donor P14 T cells were isolated from spleen and intestinal tissue
compartments as in Figure 1 at 7 days (B and C) or 21 days (D and E) post-infection.
(B and D) Quantification of the proportions (top) or absolute numbers (bottom) of control
i.v.$^-$ control vs. Eomes cKO P14 T cells in each tissue compartment at 7 days (B) or 21
days (D) post-infection.

(C and E) Representative flow cytometry plots (top) and bar graphs (bottom) indicating frequencies of control vs. Eomes cKO intestinal P14 T cells expressing CD69 and CD103 at 7 days (C) or 21 days (E) post-infection.

Data are represented as mean ± SEM. Paired *t*-test. *p<0.05, **p<0.01, ***p<0.001 ****p<0.0001. Data are representative of 3 independent experiments with n=5–6 mice per experiment.

See also Figures S5 and S6.
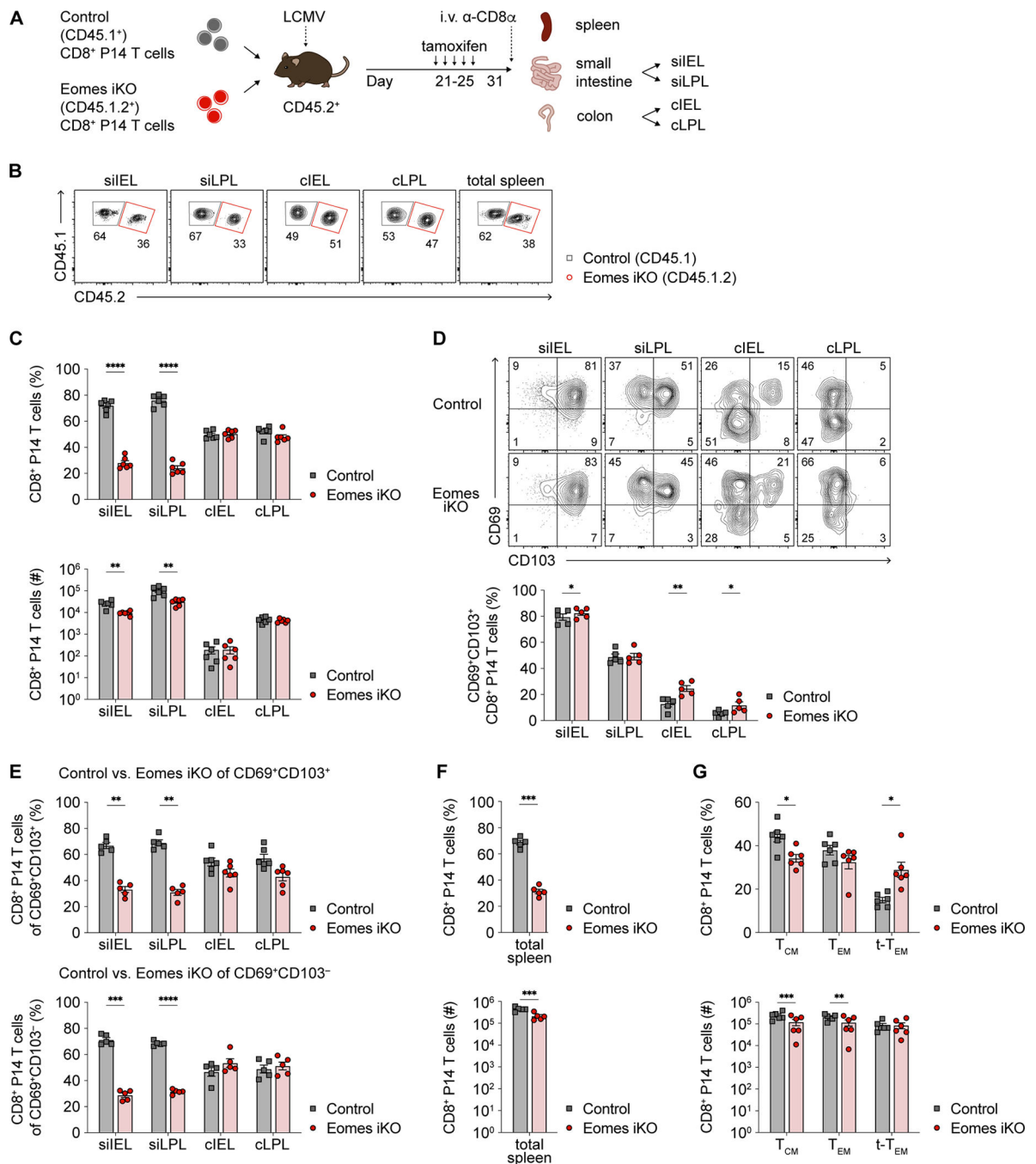
Figure 6. Eomes plays a critical role in maintenance of established SI CD8$^+$ T$_{RM}$ cells.
(A) Experimental design. CD8$^+$ T cells from congenic control and *Eomes*$^{fl/fl}$*Ert2-Cre*$^+$ (Eomes iKO) P14 mice were adoptively co-transferred at 1:1 ratio into recipients subsequently infected with LCMV. Mice received tamoxifen i.p. once daily x 5 doses starting at day 21 post-infection. Spleen and intestinal P14 T cells were harvested >10 days later.

(B and C) Representative flow cytometry plots (B) and quantification (C) of the proportions (top) or absolute numbers (bottom) of i.v.⁻ control vs. Eomes iKO P14 T cells in each intestinal tissue compartment.

(D) Representative flow cytometry plots (top) and bar graphs (bottom) indicating frequencies of control vs. Eomes iKO intestinal P14 T cells expressing CD69 and CD103.

(E) Proportions of control vs. Eomes iKO P14 T_{RM} cells among CD69$^+$CD103$^+$ (top) or CD69$^+$CD103$^-$ (bottom) subpopulations.

(F) Frequencies (top) or absolute numbers (bottom) of total control vs. Eomes iKO P14 T cells in the spleen.

(G) Bar graphs indicating the frequencies (top) or absolute numbers (bottom) of control vs. Eomes iKO T_{CM} (CD62L^{hi}CD127^{hi}), T_{EM} (CD62L^{lo}CD127^{hi}), and t-T_{EM} (CD62L^{lo}CD127^{lo}) cells.

Data are represented as mean ± SEM. Paired t-test. *p<0.05, **p<0.01, ***p<0.001 ****p<0.0001. Data are representative of 3 independent experiments with n=5–6 mice per experiment.

See also Figure S7.
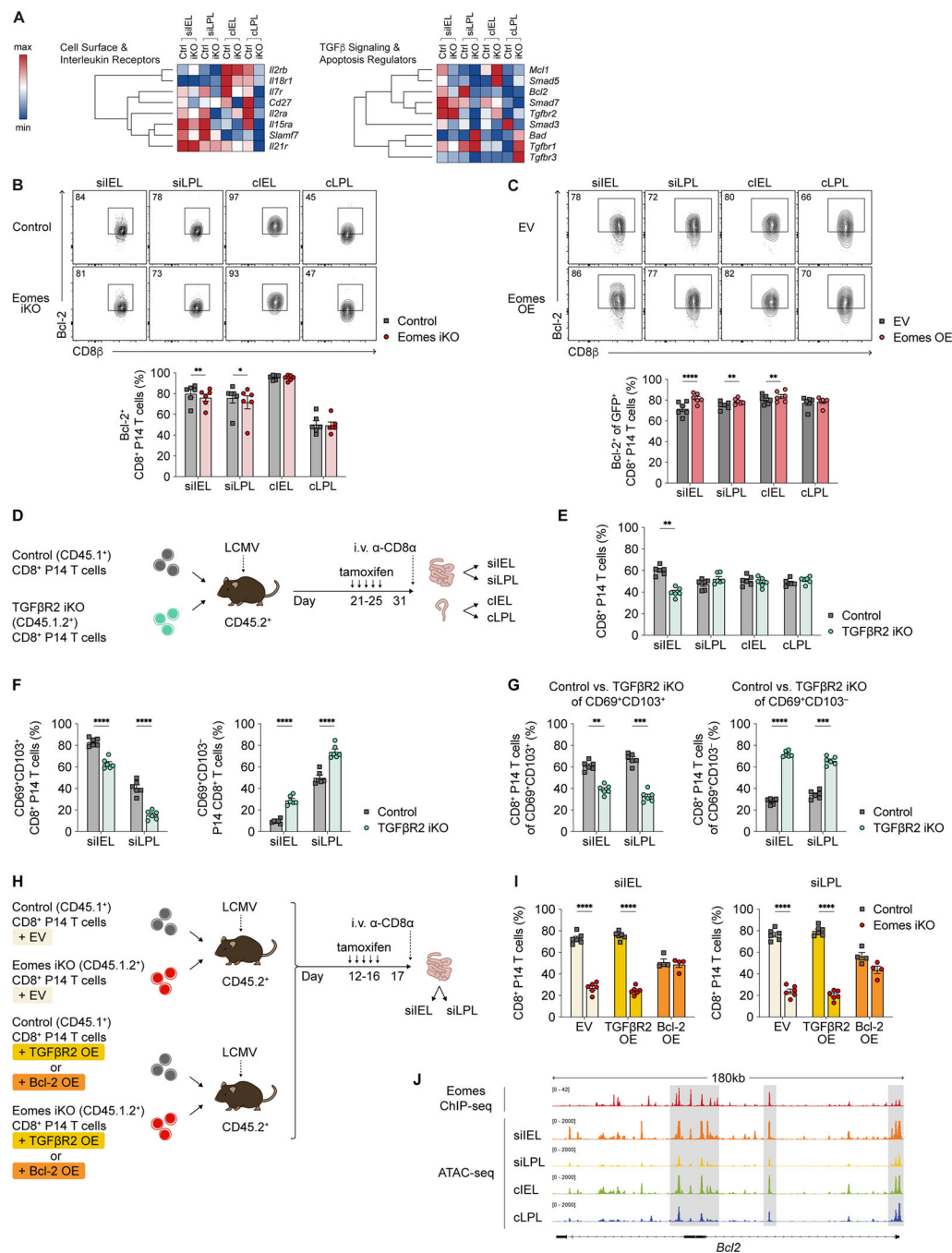
Figure 7. Eomes promotes SI CD8$^+$ T$_{RM}$ cell maintenance, in part, through effects on Bcl-2.

(A) Relative expression of selected genes derived using CITE-seq data from control vs. *Eomes*$^{fl/fl}$*Ert2-Cre*$^+$ (Eomes iKO) P14 T cells, represented as hierarchically clustered summary heatmaps; rows represent individual genes and columns represent P14 T cells from each of the 4 intestinal tissue compartments.

(B) Representative flow cytometry plots (top) and bar graphs displaying the frequencies of i.v.$^-$ control vs. Eomes iKO intestinal P14 T cells expressing Bcl-2.

(C) Representative flow cytometry plots (top) and bar graphs representing frequencies of adoptively co-transferred empty vector (EV)- vs. Eomes overexpression (OE)-transduced intestinal P14 T cells expressing Bcl-2 at day 7 following LCMV infection.

(D) Experimental design. CD8^{+} T cells from congenic control or *Tgfbr2*^{fl/fl}*Ert2-Cre*^{+} (TGFβR2 iKO) P14 mice were adoptively co-transferred at a 1:1 ratio into recipients subsequently infected with LCMV, followed by treatment with tamoxifen as in Figure 6A.

(E and F) Bar graphs representing frequencies of total (E), CD69^{+}CD103^{+} (F, left), or CD69^{+}CD103^{−} (F, right) control vs. TGFβR2 iKO i.v.[−] intestinal P14 T cells.

(H) Experimental design. CD8^{+} T cells from control (CD45.1^{+}) or Eomes iKO (CD45.1.2^{+}) P14 mice were activated and transduced with EV, TGFβR2 OE, or Bcl-2 OE constructs. Cells were mixed adoptively co-transferred at a 1:1 into CD45.2[+] recipients subsequently infected with LCMV, followed by treatment with tamoxifen as in Figure 6A.

(I) Bar graphs representing frequencies of EV-transduced control vs. Eomes iKO P14 T cells (left); TGFβR2 OE-transduced control vs. Eomes iKO P14 T cells (middle); and Bcl-2 OE-transduced control vs. Eomes iKO P14 T cells (right) in the siIEL and siLPL tissue compartments.

(J) CD45.1[+] intestinal P14 T cells were isolated from CD45.2[+] recipient mice infected with LCMV 21 days prior, FACS-purified, and processed for scATAC-seq. Tracks representing Eomes ChIP-seq (top) and scATAC-seq peaks for each of the four intestinal tissue compartments (bottom) are shown for *Bcl2.*

Data are represented as mean ± SEM. Paired *t*-test. *p<0.05, **p<0.01, ***p<0.001 ****p<0.0001. Data are representative of 3 independent experiments with n=5–6 mice per experiment.

See also Figure S7 and Table S7.

KEY RESOURCE TABLE

REAGENT or RESOURCE	SOURCE	IDENTIFIER
Antibodies		
Bcl-2 (BCL/10C4; FITC)	BioLegend	Cat#633504; RRID: AB_2028394
Bcl-2 (BCL/10C4; AF647)	BioLegend	Cat#633510; RRID: AB_2274702
CCR6 (29-2L17; PE/Dazzle 594)	BioLegend	Cat#129822; RRID: AB_2687019
CCR9 (CW-1.2; FITC)	BioLegend	Cat#128706; RRID: AB_1186167
CCR9 (CW-1.2; PE-Cy7)	BioLegend	Cat#128712; RRID: AB_10933082
CD8α (clone: 53-6.7; BV510)	BioLegend	Cat#100752; RRID: AB_2563057
CD8α (clone: 53-6.7; BV570)	BioLegend	Cat#100740; RRID: AB_2563055
CD8β (clone TS156.7.7; PE/Dazzle 594)	BioLegend	Cat#126622; RRID: AB_2632630
CD8β (clone TS156.7.7; PerCP/Cy5.5)	BioLegend	Cat#126610; RRID: AB_2260149
CD8β (clone TS156.7.7; BV421)	BioLegend	Cat#126629; RRID: AB_2800620
CD8β (clone TS156.7.7; BV510)	BioLegend	Cat#126631; RRID: AB_2800621
CD27 (clone LG.3A10; BV510)	BioLegend	Cat#124229; RRID: AB_2565795
CD27 (clone LG.3A10; BV605)	BioLegend	Cat#124249; RRID: AB_2860657
CD27 (clone LG.3A10; BV785)	BioLegend	Cat#124241; RRID: AB_2800595
CD29 (clone HMβ1-1; PerCP/Cy5.5)	BioLegend	Cat#102228; RRID: AB_2572079
CD38 (clone 90; BV421)	BioLegend	Cat#102732; RRID: AB_2734153
CD44 (clone IM7; BV421)	BioLegend	Cat#103040; RRID: AB_2616903
CD44 (clone IM7; BV650)	BioLegend	Cat#103049; RRID: AB_2562600
CD44 (clone IM7; BV785)	BioLegend	Cat#103059; RRID: AB_2571953
CD45.1 (clone A20; FITC)	BioLegend	Cat#110706; RRID: AB_313495
CD45.1 (clone A20; BV421)	BioLegend	Cat#110732; RRID: AB_2562563
CD45.1 (clone A20; BV510)	BioLegend	Cat#110741; RRID: AB_2563378
CD45.1 (clone A20; BV605)	BioLegend	Cat#110738; RRID: AB_2562565
CD45.1 (clone A20; BV650)	BioLegend	Cat#110736; RRID: AB_2562564
CD45.2 (clone 104; FITC)	BioLegend	Cat#109806; RRID: AB_313443
CD45.2 (clone 104; BV421)	BioLegend	Cat#109832; RRID: AB_2565511
CD45.2 (clone 104; BV510)	BioLegend	Cat#109838; RRID: AB_2650900
CD45.2 (clone 104; BV605)	BioLegend	Cat#109841; RRID: AB_2563485
CD45.2 (clone 104; BV650)	BioLegend	Cat#109836; RRID: AB_2563065
CD49a (clone HMα1; APC)	BioLegend	Cat#142606; RRID: AB_2562253
CD49d (clone R1-2; PE-Cy7)	BioLegend	Cat#103618; RRID: AB_2563700
CD62L (clone MEL-14; APC)	BioLegend	Cat#104412; RRID: AB_313099
CD62L (clone MEL-14; BV421)	BioLegend	Cat#104436; RRID: AB_2562560
CD62L (clone MEL-14; BV605)	BioLegend	Cat#104438; RRID: AB_2563058
CD62L (clone MEL-14; BV650)	BioLegend	Cat#104453; RRID: AB_2800559
CD62L (clone MEL-14; BV785)	BioLegend	Cat#104440; RRID: AB_2629685
CD69 (clone H1.2F3; PE/Dazzle 594)	BioLegend	Cat#104536; RRID: AB_2565583

REAGENT or RESOURCE	SOURCE	IDENTIFIER
CD69 (clone H1.2F3; BV421)	BioLegend	Cat#104528; RRID: AB_2562328
CD69 (clone H1.2F3; BV605)	BioLegend	Cat#104530; RRID: AB_2563062
CD69 (clone H1.2F3; BV650)	BioLegend	Cat#104541; RRID: AB_2616934
CD69 (clone H1.2F3; BV785)	BioLegend	Cat#104543; RRID: AB_2629640
CD103 (clone 2E7; PE)	BioLegend	Cat#121406; RRID: AB_1133989
CD103 (clone 2E7; BV421)	BioLegend	Cat#121422; RRID: AB_2562901
CD103 (clone 2E7; BV605)	BioLegend	Cat#121433; RRID: AB_2629724
CD103 (clone 2E7; BV785)	BioLegend	Cat#121439; RRID: AB_2800588
CD122 (clone TM-β1; PE/Dazzle 594)	BioLegend	Cat#123218; RRID: AB_2572180
CD127 (clone A7R34; FITC)	BioLegend	Cat#135008; RRID: AB_1937232
CD127 (clone A7R34; PE)	BioLegend	Cat#135010; RRID: AB_1937251
CD127 (clone A7R34; APC)	BioLegend	Cat#135012; RRID: AB_1937216
CD127 (clone A7R34; BV421)	BioLegend	Cat#135024; RRID: AB_11218800
CD127 (clone A7R34; BV605)	BioLegend	Cat#135041; RRID: AB_2572047
CD127 (clone A7R34; BV650)	BioLegend	Cat#135043; RRID: AB_2629681
CD127 (clone A7R34; BV785)	BioLegend	Cat#135037; RRID: AB_2565269
CD160 (clone 7H1; PerCP/Cy5.5)	BioLegend	Cat#143008; RRID: AB_2562676
CD160 (clone 7H1; PE-Cy7)	BioLegend	Cat#143010; RRID: AB_2562678
CD314 (clone CX5; PE)	BioLegend	Cat#130208; RRID: AB_1227712
CD314 (clone CX5; PE/Dazzle 594)	BioLegend	Cat#130214; RRID: AB_2728148
CXCR3 (clone CXCR3-173; PE/Dazzle 594)	BioLegend	Cat#126534; RRID: AB_2566563
CXCR3 (clone CXCR3-173; PerCP/Cy5.5)	BioLegend	Cat#126514; RRID: AB_1186015
CXCR3 (clone CXCR3-173; BV605)	BioLegend	Cat#126523; RRID: AB_2561353
CXCR3 (clone CXCR3-173; BV650)	BioLegend	Cat#126531; RRID: AB_2563160
CXCR4 (clone L276F12; BV421)	BioLegend	Cat #146511; RRID: AB_2562788
Eomes (clone Dan11mag; PE-Cy7)	ThermoFisher	Cat #25-4875-82; RRID: AB_2573454
GzmA (clone GzA-3G8.5; PE)	ThermoFisher	Cat #12-5831-82; RRID: AB_2572631
GzmA (clone GzA-3G8.5; PE-Cy7)	ThermoFisher	Cat #25-5831-82; RRID: AB_2573476
GzmA (clone GzA-3G8.5; APC)	ThermoFisher	Cat #17-5831-82; RRID: AB_2573228
GzmB (clone GB11; FITC)	BioLegend	Cat #515403; RRID: AB_2114575
GzmB (clone QA16A02; PE/Dazzle 594)	BioLegend	Cat #372216; RRID: AB_2728383
GzmB (clone GB11; AlexaFluor 647)	BioLegend	Cat #515406; RRID: AB_2566333
GzmB (clone QA16A02; APC)	BioLegend	Cat #372204; RRID: AB_2687028
GzmB (clone QA18A28; BV421)	BioLegend	Cat #396414; RRID: AB_2810603
IFNγ (clone XMG1.2; PE/Dazzle 594)	BioLegend	Cat #505846; RRID: AB_2563980
IFNγ (clone XMG1.2; BV785)	BioLegend	Cat #505838; RRID: AB_2629667
IL-2 (clone JES6-5H4; BV421)	BioLegend	Cat #503826; RRID: AB_2650897
IL-2 (clone JES6-5H4; BV605)	BioLegend	Cat #503829; RRID: AB_11204084
IL-18R (clone A17071D; AlexaFluor 647)	BioLegend	Cat #157908; RRID: AB_2876539

REAGENT or RESOURCE	SOURCE	IDENTIFIER
Integrin β7 (clone FIB504; FITC)	BioLegend	Cat #321213; RRID: AB_830857
Integrin β7 (clone FIB504; PE/Dazzle 594)	BioLegend	Cat #321226; RRID: AB_2715983
Ki67 (clone 16A8; PE)	BioLegend	Cat #652404; RRID: AB_2561525
Ki67 (clone 16A8; PE/Dazzle 594)	BioLegend	Cat #652428; RRID: AB_2632696
Ki67 (clone 16A8; PerCP/Cy5.5)	BioLegend	Cat #652424; RRID: AB_2629531
Ki67 (clone 16A8; BV421)	BioLegend	Cat #652411; RRID: AB_2562663
KLRG1 (clone 2F1/KLRG1; PE/Dazzle 594)	BioLegend	Cat #138424; RRID: AB_2564051
KLRG1 (clone 2F1/KLRG1; PerCp/Cy5.5)	BioLegend	Cat #138418; RRID: AB_2563015
KLRG1 (clone 2F1/KLRG1; BV421)	BioLegend	Cat #138414; RRID: AB_2565613
KLRG1 (clone 2F1/KLRG1; BV605)	BioLegend	Cat #138419; RRID: AB_2563357
KLRG1 (clone 2F1/KLRG1; BV785)	BioLegend	Cat #138429; RRID: AB_2629749
Ly6C (clone HK1.4; BV605)	BioLegend	Cat #128036; RRID: AB_2562353
Ly108 (clone 13G3; BV421)	BD Biosciences	Cat #740090; RRID: AB_2739850
P2RX7 (clone 1F11; PerCP/Cy5.5)	BioLegend	Cat #148710; RRID: AB_2728183
P2RX7 (clone 1F11; PE-Cy7)	BioLegend	Cat #148708; RRID: AB_2721686
P2RX7 (clone 1F11; APC)	BioLegend	Cat #148706; RRID: AB_2650954
T-bet (clone 4B10; BV785)	BioLegend	Cat #644835; RRID: AB_2721566
TNFα (clone MP6-XT22; BV650)	BioLegend	Cat #506333; RRID: AB_2562450
T-reg protector (anti-ARTC2 Nanobody) (clone S+16a)	BioLegend	Cat#149802; RRID: AB_2565494
Goat anti-Hamster IgG (H+L) Secondary Antibody	ThermoFisher	Cat#31115; RRID: AB_228247
InVivoMAb anti-mouse CD3 (clone 17A2)	BioXCell	Cat#BE0002; RRID: AB_1107630
InVivoMAb anti-mouse CD28 (clone PV-1)	BioXCell	Cat#BE0015-5; RRID: AB_1107628
InVivoMAb anti-mouse/human IL-7 (clone M25)	BioXCell	Cat #BE0048; RRID: AB_1107711
TotalSeq™-A0214 anti-human/mouse integrin β7 Antibody	BioLegend	Cat#321227; RRID: AB_2750504
TotalSeq™-A0201 anti-mouse CD103 Antibody	BioLegend	Cat#121437; RRID: AB_2750349
TotalSeq™-A0198 anti-mouse CD127 (IL-7Rα) Antibody	BioLegend	Cat#135045; RRID: AB_2750009
TotalSeq™-A0195 anti-mouse CD134 (OX-40) Antibody	BioLegend	Cat#119426; RRID: AB_2750376
TotalSeq™-A0194 anti-mouse CD137 Antibody	BioLegend	Cat#106111; RRID: AB_2783048
TotalSeq™-A1006 anti-mouse CD160 Antibody	BioLegend	Cat#143013; RRID: AB_2832512
TotalSeq™-A0444 anti-mouse CD184 (CXCR4) Antibody	BioLegend	Cat#146520; RRID: AB_2800682
TotalSeq™-A0846 anti-mouse CD185 (CXCR5) Antibody	BioLegend	Cat#145535; RRID: AB_2800681
TotalSeq™-A0376 anti-mouse CD195 (CCR5) Antibody	BioLegend	Cat#107019; RRID: AB_2783049
TotalSeq™-A0225 anti-mouse CD196 (CCR6) Antibody	BioLegend	Cat#129825; RRID: AB_2783083
TotalSeq™-A0854 anti-mouse CD199 (CCR9) Antibody	BioLegend	Cat#128713; RRID: AB_2832466

REAGENT or RESOURCE	SOURCE	IDENTIFIER
TotalSeq™-A0378 anti-mouse CD223 (LAG-3) Antibody	BioLegend	Cat#125229; RRID: AB_2783078
TotalSeq™-A0852 anti-mouse CD226 (DNAM-1) Antibody	BioLegend	Cat#128823; RRID AB_2810393
TotalSeq™-A0097 anti-mouse CD25 Antibody	BioLegend	Cat#102055; RRID: AB_2749982
TotalSeq™-A0191 anti-mouse/rat/human CD27 Antibody	BioLegend	Cat#124235; RRID: AB_2750344
TotalSeq™-A0190 anti-mouse CD274 (B7-H1, PD-L1) Antibody	BioLegend	Cat#153604; RRID: AB_2783125
TotalSeq™-A0004 anti-mouse CD279 (PD-1) Antibody	BioLegend	Cat#109123; RRID: AB_2734169
TotalSeq™-A0570 anti-mouse/rat CD29 Antibody	BioLegend	Cat#102233; RRID: AB_2783042
TotalSeq™-A0184 anti-mouse CD335 (NKp46) Antibody	BioLegend	Cat#137633; RRID: AB_2734199
TotalSeq™-A0193 anti-mouse CD357 (GITR) Antibody	BioLegend	Cat#126319; RRID: AB_2734195
TotalSeq™-A0003 anti-mouse CD366 (Tim-3) Antibody	BioLegend	Cat#119729; RRID: AB_2734178
TotalSeq™-A0110 anti-mouse CD43 Antibody	BioLegend	Cat#143211; RRID: AB_2750541
TotalSeq™-A0073 anti-mouse/human CD44 Antibody	BioLegend	Cat#103045; RRID: AB_2734154
TotalSeq™-A0850 anti-mouse CD49a Antibody	BioLegend	Cat#142613; RRID: AB_2800659
TotalSeq™-A0078 anti-mouse CD49d Antibody	BioLegend	Cat#103623; RRID: AB_2734159
TotalSeq™-A0112 anti-mouse CD62L Antibody	BioLegend	Cat#104451; RRID: AB_2750364
TotalSeq™-A0197 anti-mouse CD69 Antibody	BioLegend	Cat#104546; RRID: AB_2750539
TotalSeq™-A0230 anti-mouse CD8b (Ly-3) Antibody	BioLegend	Cat#126623; RRID: AB_2800615
TotalSeq™-A1009 anti-mouse CD94 Antibody	BioLegend	Cat#105515; RRID: AB_2819808
TotalSeq™-A0847 anti-mouse CD278 (ICOS) Antibody	BioLegend	Cat#117409; RRID: AB_2800585
TotalSeq™-A0563 anti-mouse CX3CR1 Antibody	BioLegend	Cat#149041; RRID: AB_2783121
TotalSeq™-A0250 anti-mouse/human KLRG1 (MAFA) Antibody	BioLegend	Cat#138431; RRID: AB_2800648
TotalSeq™-A0930 anti-mouse Ly108 Antibody	BioLegend	Cat#134611; RRID: AB_2888706
TotalSeq™-A0824 anti-mouse P2X7R Antibody	BioLegend	Cat#148711; RRID: AB_200683
TotalSeq™-A0848 anti-mouse TIGIT (Vstm3) Antibody	BioLegend	Cat#142115; RRID: AB_2800656
TotalSeq™-A0905 anti-mouse CD107a (LAMP-1) Antibody	BioLegend	Cat#121635; RRID: AB_2810369
TotalSeq™-A0839 anti-mouse Ly49H Antibody	BioLegend	Cat#144715; RRID: AB_2814049
TotalSeq™-A0111 anti-mouse CD5 Antibody	BioLegend	Cat#100637; RRID: AB_2749985
TotalSeq™-A1019 anti-mouse CD215 (IL-15Rα) Antibody	BioLegend	Cat#153507; RRID: AB_2832537
TotalSeq™-A0557 anti-mouse CD38 Antibody	BioLegend	Cat#102733; RRID: AB_2750556
TotalSeq™-A0835 anti-mouse CD314 (NKG2D) Antibody	BioLegend	Cat#130215; RRID: AB_2814023

REAGENT or RESOURCE	SOURCE	IDENTIFIER
TotalSeq™-A0834 anti-mouse CD39 Antibody	BioLegend	Cat#143813; RRID: AB_2800669
TotalSeq™-A0013 anti-mouse Ly-6C Antibody	BioLegend	Cat#128047; RRID: AB_2749961
TotalSeq™-A0885 anti-mouse CD270 (HVEM) Antibody	BioLegend	Cat#136307; RRID: AB_2810403
TotalSeq™-A0989 anti-mouse CD98 (4F2) Antibody	BioLegend	Cat#128223; RRID: AB_2876456
TotalSeq™-A0388 anti-mouse CD152 Antibody	BioLegend	Cat#106325; RRID: AB_2876417
TotalSeq™-A0883 anti-mouse CD26 (DPP-4) Antibody	BioLegend	Cat#137811; RRID: AB_2810405
TotalSeq™-A0157 anti-mouse CD45.2 Antibody	BioLegend	Cat#109853; RRID: AB_2783051
TotalSeq™-A0178 anti-mouse CD45.1 Antibody	BioLegend	Cat#110753; RRID: AB_2800573
TotalSeq™-A0911 anti-phycoerythrin (PE) Antibody	BioLegend	Cat#408109; RRID: AB_2820078
TotalSeq™-A0227 anti-mouse CD122 (IL-2Rb)	BioLegend	Custom
Bacterial and viral strains		
LCMV-Armstrong	This paper	N/A
Bcl-2 overexpression retrovirus	This paper	N/A
Eomes overexpression retrovirus	This paper	N/A
TGFβRII overexpression retrovirus	This paper	N/A
Empty vector retrovirus	This paper	N/A
shRNA non-target retrovirus	This paper	N/A
shRNA P2RX7 retrovirus	This paper	N/A
Chemicals, peptides, and recombinant proteins		
Recombinant Murine IL-7	PeproTech	Cat#217-17
TransIT-LT1 Transfection Reagent	Mirus	Cat#MIR 23000
eBioscience Fixable Viability Dye eFluor 780	ThermoFisher	Cat#65-0865-18
eBioscience Fixation/Perm Diluent	ThermoFisher	Cat#00-5223-56
Fixation/Permeabilization concentrate	ThermoFIsher	Cat#00-5123-43
Permeabilization Buffer 10×	ThermoFisher	Cat#00-8333-56
Paraformaldehyde 16% Aqueous solution, EM grade	Fisher Scientific	Cat#50-980-487
Fetal Bovine Serum	Genesee Scientific	Cat#25-525H
Ethylenediaminetetraacetic acid	Fisher Scientific	Cat#BP2482100
Percoll	Sigma Aldrich	Cat#P1644
L-glutamine 200 mM (100×)	ThermoFisher	Cat#25030-081
Penicillin-Streptomycin (10,000 U/mL)	ThermoFisher	Cat#15140-122
HEPES	Sigma Aldrich	Cat#H3375
4-hydroxytamoxifen	Sigma Aldrich	Cat#T176
Sunflower seed oil	Sigma Aldrich	Cat#S5007
Isoflurane	Vetone	Cat#502017
Ethyl alcohol	Sigma Aldrich	Cat#E7023

REAGENT or RESOURCE	SOURCE	IDENTIFIER
Dulbecco's Modified Eagle Medium	ThermoFisher	Cat#11965-092
Collagenase from Clostridium hystolyticum (Type IV)	Sigma Aldrich	Cat#C5138
Dithiothretiol (DTT)	ThermoFisher	Cat#R0861
DNase I, grade II, from bovine pancreas	Roche	Cat#10104159001
Hank's Balanced Salt Solution	Corning	Cat#21-021-CV
Dulbecco's Phosphate-Buffered Saline	Corning	Cat#21-031-CM
Critical commercial assays		
CD8+ T Cell Isolation Kit, mouse	Miltenyi	Cat#130-104-075
Chromium Next GEM Single Cell 3' GEM, Library & Gel Bead Kit v3.1	10X Genomics	Cat#PN-1000121
Chromium Next GEM Single Cell ATAC Library & Gel Bead Kit v1.1	10X Genomics	Cat#PN-1000175
Chromium Next GEM Chip G Single Cell Kit, 16 rxns	10X Genomics	Cat#PN-1000127
Chromium Next GEM Chip H Single Cell Kit, 16 rxns	10X Genomics	Cat#PN-1000162
Deposited data		
CITE-seq data	This paper	GEO: GSE205942
scATAC-seq data	This paper	GEO: GSE205942
Teichmann Gut Atlas - T/NK cells	Elmentaite et al., 2021	ArrayExpress: E-MTAB-9532
Experimental models: Cell lines		
Platinum-E (Plat-E) cell line	Cell Biolabs, Inc.	Cat#RV-101; RRID: CVCL_B488
BHK-21 (C13)	ATCC	Cat#CCL-10; RRID: CVCL_1915
Experimental models: Organisms/strains		
Mouse: B6.SJL-Ptprc^a Pepc^b/BoyJ (CD45.1)	Jackson Laboratory	RRID: IMSR_JAX:002014
Mouse: C57BL/6J (CD45.2)	Jackson Laboratory	RRID: IMSR_JAX:000664
Mouse: B6.Cg-Tcra^{tm1Mom} Tg(TcrLCMV)327Sdz (P14)	Jackson Laboratory	RRID: MMRRC_037394-MU
Mouse: B6.129S1(Cg)-Eomes$^{tm1.1Bflu}$/J (Eomes fl/fl)	Jackson Laboratory	RRID: IMSR_JAX:017293
Mouse: B6.Cg-Tg(Cd4-cre)1Cwi/BfluJ (CD4-Cre)	Jackson Laboratory	RRID: IMSR_JAX:022071
Mouse: B6.Cg-Tg(CAG-cre/Esr1*)5Amc/J (ER-Cre)	Jackson Laboratory	RRID: IMSR_JAX:004682
Mouse: B6;129-Tgfbr2^{tm1Karl}/J (TGFβR2 fl/fl)	Jackson Laboratory	RRID: IMSR_JAX:012603
Recombinant DNA		
pCL-Eco Retrovirus packaging vector	Addgene	RRID: Addgene_12371
pMIG Vector	Addgene	RRID: Addgene_9044
pMIG Eomes Vector	Dr. Steven Reiner	N/A
pMIG Bcl-2 Vector	Dr. Michael Croft	RRID: Addgene_8793

REAGENT or RESOURCE	SOURCE	IDENTIFIER
pMIG TGFβRII Vector	Dr. Wanjun Chen	N/A
pLMPd-Ametrine	Transomic	shRNA retroviral target gene set
shERWOOD UltramiR Lentiviral shRNA target gene set for gene P2RX7	Transomic	Car#TLHSU1435
Software and algorithms		
FlowJo v10.8.1	FlowJo	https://www.flowjo.com/
Prism 9	GraphPad	https://www.graphpad.com/scientific-software/prism/
Cell Ranger 6.0.1	10x Genomics	https://support.10xgenomics.com/single-cell-gene-expression/software/overview/welcome
Seurat 4.1.0.9001	Hao et al., 2021	https://satijalab.org/seurat/
Metascape	Zhou et al., 2019	https://metascape.org/
scVelo v0.2.4	Bergen et al., 2020	https://scvelo.readthedocs.io/
Signac v1.6.0	Stuart et al., 2021	https://satijalab.org/signac/
pheatmap v1.0.8 (R package)	Kolde, 2019	https://cran.r-project.org/package=pheatmap
VennDiagram v1.7.3 (R package)	Chen, 2022	https://cran.r-project.org/package=VennDiagram